

# GHASP : an $H\alpha$ kinematic survey of spiral and irregular galaxies. V. Dark matter distribution in 36 nearby spiral galaxies

Spano M.<sup>1</sup>, Marcelin M.<sup>1</sup>, Amram, P.<sup>1</sup>, Carignan C.<sup>2</sup>, Epinat B.<sup>1</sup>, Hernandez O.<sup>2</sup> <sup>★</sup>

<sup>1</sup>Laboratoire d'Astrophysique de Marseille, OAMP, 2 Place Le Verrier, 13248 Marseille Cedex 04 France

<sup>2</sup>Laboratoire d'Astrophysique Expérimentale, Université de Montréal, C.P. 6218, Succ. Centre-ville, Montréal, Qc, Canada H3C 3J7

Accepted. Received; in original form

## ABSTRACT

The results obtained from a study of the mass distribution of 36 spiral galaxies are presented. The galaxies were observed using Fabry-Perot interferometry as part of the GHASP survey. The main aim of obtaining high resolution  $H\alpha$  2D velocity fields is to define more accurately the rising part of the rotation curves which should allow to better constrain the parameters of the mass distribution. The  $H\alpha$  velocities were combined with low resolution HI data from the literature, when available. Combining the kinematical data with photometric data, mass models were derived from these rotation curves using two different functional forms for the halo: an isothermal sphere and an NFW profile. For the galaxies already modeled by other authors, the results tend to agree. Our results point at the existence of a constant density core in the center of the dark matter halos rather than a cuspy core, whatever the type of the galaxy from Sab to Im. This extends to all types the result already obtained by other authors studying dwarf and LSB galaxies but would necessitate a larger sample of galaxies to conclude more strongly. Whatever model is used (ISO or NFW), small core radius halos have higher central densities, again for all morphological types. We confirm different halo scaling laws, such as the correlations between the core radius and the central density of the halo with the absolute magnitude of a galaxy: low luminosity galaxies have small core radius and high central density. We find that the product of the central density with the core radius of the dark matter halo is nearly constant, whatever the model and whatever the absolute magnitude of the galaxy. This suggests that the halo surface density is independent from the galaxy type.

**Key words:** instrumentation: interferometers Galaxies: spiral; irregular; dwarf; Galaxies: kinematics and dynamics; Galaxies: haloes; dark matter

## 1 INTRODUCTION

Rotation curves are a fundamental tool for studying the dynamics and mass distribution in galaxies. The distribution of the total mass can then be compared with the distribution of visible light, assuming a certain mass-to-light (M/L) ratio. Observations have clearly established that dark matter is needed for explaining the rotation velocities observed in the outer parts of spirals. The dark matter is most often considered as being distributed in a spherical dark halo but its density profile, especially at small radii, is still a matter of debate (Blais-Ouellette et al. 2001, de Blok & Bosma

2002, Swaters et al. 2003, Navarro 2004, Graham et al. 2006, Kusio de Naray 2006, Hayashi et al. 2007).

However, mass models of spiral and dwarf galaxies have well-known degeneracies (Barnes et al. 2004) that prevent a unique mass decomposition, the most important being the unknown value of the stellar mass-to-light ratio (Dutton et al. 2005). Unfortunately, stellar population models (e.g. de Jong & Bell 2006) still cannot predict accurately the (M/L) values of the stellar disks based on their colors. The main problem comes from the fact that the normalization of this relation (color vs M/L) depends critically on the shape of the stellar IMF at the low mass end. It is well known that the faint stars contribute significantly to the mass but not to the luminosity and color of the stellar disks. This means

<sup>★</sup> Based on observations collected at the Observatoire de Haute Provence

that it will prove difficult to tighten this relation and lessen the effect of the disk-halo degeneracy.

Cosmological numerical simulations favor cuspy dark halos, although the value of the inner slope  $\gamma$  of the radial density profile, where  $\rho \propto r^{-\gamma}$  (see equation 6 of section 4) depends on the authors, with  $\gamma = -1.5$  for Moore et al. 1999 as well as Fukushige & Makino 2001 or  $-1.0$  for Navarro, Frenk & White 1997 (hereafter NFW). Recent simulations (Graham et al. 2006) have extrapolated inner logarithmic profile slope ranging from  $-0.2$  to  $-1.5$ , with a typical value at  $0.1$  kpc around  $-0.7$ .

Most observers conclude however that  $\gamma$  is closer to  $0.0$  than to  $-1.0$  and that mass models give better results with an isothermal (or pseudo-isothermal) sphere halo rather than a NFW profile (e.g. Blais-Ouellette et al. 2001, de Blok & Bosma 2002, Swaters et al. 2003, de Blok et al. 2003, de Blok 2005, Kassin et al. 2006a). Most of these observations are based on the rotation curves of dwarf and Low Surface Brightness (LSB) galaxies (Kuzio de Naray et al. 2006). It is still unclear if this is true also for High Surface Brightness (HSB) systems and for all morphological types.

One problem in this cusp-core debate is that numerical simulations mainly predict the halo density profile shape at the time of formation while galaxies are observed after many Gyrs of evolution. The problem is that internal dynamics and interaction between the dark halo and the luminous disk (e.g. adiabatic contraction: Dutton et al. 2005) and interaction with the environment (Maccio et al. 2007) may have altered the shape of the halo density profile.

Moreover, the shape of the gravitational potential in CDM halos may explain the core-like halo density profiles seen in LSB systems. Hayashi et al. 2007 suggest that galactic disks may be forming in elliptical gravitational potential. This could result in significant non-circular motions in systems such as LSBs which would mimic constant density cores. Thus, taking into account the 3D shape of the dark mass distribution could reconcile the constant density cores observed in LSBs with the predicted cuspy mass profiles of CDM halos.

Finally, it is unclear if CDM simulations, mainly obtained to compare with the large scale structure, have sufficient resolution to reliably probe the kpc scales necessary to compare with the observationally derived dark matter halo density profiles on the scale of a few halo core radii. As discussed by Navarro (2004), unfortunately rotation curves constraints are strongest where numerical simulations are the least reliable. In fact, rotation curves are usually compared with extrapolations of the simulation data that rely heavily on the applicability and accuracy of fitting formulae such as the NFW profile to regions that may be compromised by numerical artifact. This is especially true for LSB and dwarf galaxies (for instance Dutton et al. 2005).

Blais-Ouellette et al. 1999 and Barnes et al. 2004 have shown the necessity of optical integral field spectroscopy to accurately determine the rotation curves in the inner parts of spiral and dwarf galaxies, for which the HI data are affected by beam smearing (Swaters et al. 2000, van den Bosch et al. 2000). While the use of two-dimensional data does not necessarily alter the halo parameters derived from optical long-slit data it however decreases the uncertainties by roughly a factor of 2 (de Naray et al. 2006). Blais-Ouellette et al. 2001 and Blais-Ouellette et al. 2004 also pointed out

the great sensitivity of the mass distribution parameters to the inner rotation curve. The ideal rotation curve will therefore combine high resolution optical data, for the inner part, with radio data, for the outer part extending well beyond the luminous disk.

## 2 THE SAMPLE

The sample of 36 galaxies studied in this paper is composed of nearby galaxies observed for the GHASP survey. These 36 galaxies are simply the GHASP galaxies already reduced (113 out of a total of  $\sim 200$  observed galaxies) for which there is photometry available in the literature and for which we could draw an acceptable rotation curve at  $H\alpha$  wavelength. Half of them has been already published and another half has been reduced recently and only available on the GHASP website. For 19 of them, the velocity fields and rotation curves have been published in Garrido et al. 2002, 2003, 2004 and 2005; 17 other galaxies (observed in 2004) have been reduced recently and the data will be published later (Epinat et al. 2008). However, their monochromatic images, velocity fields and rotation curves are already available on the GHASP web site : <http://www.oamp.fr/interferometrie/GHASP/ghasp.html>.

Eight other galaxies from the same observing run (2004) are also presented on the GHASP website but they are not analyzed here, because no photometry is available (UGC 4770, 5319, 5373 and IC 2542) or because of problems with the rotation curve (UGC 4393, 6277, 8863 and 9358), as explained in the next paragraph.

The GHASP survey provides high resolution velocity fields of nearby galaxies at the  $H\alpha$  wavelength. For the analysis done in this paper, we selected the galaxies for which photometric data were available in the literature. Then we excluded all the galaxies with strong differences between the red and the blue side of the rotation curve or displaying high velocity dispersions hence difficult to fit properly with mass models. These galaxies are: UGC 4278 (seen edge-on), UGC 4305 (strong velocity dispersion and counter rotation in the center), UGC 4393 (anomalous rotation curve with counter rotation in the center), UGC 5414 (strong dispersion and asymmetry of the velocities between receding and approaching side), UGC 6277 (rotation curve abnormally flat in the central part), UGC 7971 (strong dispersion and asymmetry of the velocities between receding and approaching side), UGC 8863 (not enough  $H\alpha$  emission to get a correct rotation curve) and UGC 9358 (very strong asymmetry : plateau immediately reached for the approaching side and solid body rotation for the receding side).

In Table 1, the morphological type is completed by an additional mention: LSB for low surface brightness galaxies and dS for dwarf spirals. We have adopted the same criterion as Pizzella et al. 2005, considering that LSB have a disk with a central face-on surface brightness  $\mu_B \geq 22.6$  mag/arcsec<sup>2</sup>. The criteria for dwarf spirals are those defined by Schombert et al. 1995. We thus find that 9 galaxies of our sample are LSB and 5 are dwarf spirals, UGC 2034 and 5272 being both. All of them are late type galaxies: 2 Scd, 2 Sdm, 1 Sm and 4 Im for the 9 LSB, 1 Sd, 1 Sm and 3 Im for the 5 dS.

Since there are only 9 LSB and 5 dS in our sample, it is not possible however to make any significant study for

**Table 1.** Data used for the analysis of our sample.

N° UGC (1)	N° NGC (2)	Type (3)	Distance Mpc (4)	$M_B$ (5)	$D_{25/2}$ arcmin (6)	b/a (7)	$i$ ° (8)	$A_G(R)$ (9)	$\Sigma_{HI}$ (10)	HI RC (11)	Phot./Band (12)	h kpc (13)	Rlast kpc (14)
2034		Im/LSB/dS	10.1 (Sw02)	-16.41	1.3	0.79	19	0.15	Sw02a	Sw99	Sw02b/R	1.26±0.02	5.9
2455	1156	IB(s)m	7.8 (Sw02)	-18.05	1.7	0.68	51	0.60	Sw02a	Sw99	Sw02b/R	0.87±0.07	4.5
2503	1169	SABb	34.4 (Koo06)	-21.82	2.1	0.74	53	0.58		vD94	vD94/R	5.14±0.01	38
3876		SA(s)d	14.5 (Jam04)	-17.65	1.1	0.58	59	0.12			Cou96/R	1.37±0.02	5.1
4256	2532	SAB(rs)c	71.7	-21.65	1.1	0.83	38	0.14			Dej94/R	5.15±0.01	18
4274	2537	SB(s)m	6.9 (Kar04)	-17.17	0.9	0.85	40	0.14	Sw02a	S02	Sw02b/R	0.68±0.17	4.0
4325	2552	SA(s)m	10.1 (Sw02)	-17.76	1.7	0.66	41	0.12	Sw02a	Sw99	Sw02b/R	1.73±0.01	7.1
4456		SA(rs)c	74.0	-20.93	0.9	0.89	27	0.10			OHP120/R	4.71±0.01	29
4499		SABdm	13.0	-17.36	1.3	0.74	50	0.09	Sw02a	Sw99	Sw02b/R	1.40±0.02	8.5
4555	2649	SAB(rs)bc	58.0	-20.91	0.8	0.95	35	0.09			OHP120/R	4.25±0.01	17
5175	2977	Sb	44.1	-20.62	0.9	0.44	62	0.08			OHP120/R	2.36±0.01	9.6
5272		Im/LSB/dS	7.1 (Kar04)	-15.27	1.0	0.38	59	0.06	Sw02a	Sw99	Sw02b/R	0.89±0.12	2.2
5279	3026	Im/LSB	21.2	-18.53	1.3	0.30	78	0.06			OHP120/R	2.44±0.01	8.8
5721	3274	SABd/dS	6.5 (Kar04)	-16.38	1.1	0.48	61	0.06	Sw02a	Sw99	Sw02b/R	0.43±0.22	7.1
5789	3319	SB(rs)cd/LSB	14.1 (Saha06)	-19.62	3.1	0.55	65	0.04	Mo98	Mo98	Kas06/R	6.19±0.01	24
5842	3346	SB(rs)cd	15.2 (Sha01)	-18.67	1.4	0.87	47	0.07			Dej94/R	1.75±0.02	5.8
6537	3726	SAB(r)c	14.3	-20.11	3.1	0.69	50	0.04	Ver01	Ver01	Kas06/R	3.07±0.01	26
6778	3893	SAB(rs)c	15.5 (Shap01)	-20.27	0.5	0.62	49	0.06	Ver01	Ver01	Kas06/R	2.06±0.04	17
7045	4062	SA(s)c	11.4 (Mou06)	-19.00	2.0	0.43	69	0.07	Bro94		Kas06/R	1.89±0.01	7.6
7323	4242	SAB(s)dm	8.1 (Sw02)	-18.24	2.5	0.76	50	0.03	Sw02a	Sw99	Sw02b/R	2.04±0.01	5.9
7524	4395	SAB(s)m/LSB	4.6 (Kar04)	-17.74	6.6	0.83	46	0.05	Sw02a	Sw99	Sw02b/R	3.00±0.01	10
7699		SBcd/LSB	9.3	-17.51	1.9	0.27	78	0.03	Bro94		Jan00/R	0.67±0.16	6.3
7876	4635	SAB(s)d	12.8	-17.68	1.0	0.70	44	0.07			Dej94/R	1.17±0.04	3.0
7901	4651	SA(rs)c	20.6 (Sha01)	-20.53	2.0	0.66	53	0.07	War88		Dej94/R	2.69±0.01	15
8490	5204	SA(s)m/dS	4.7 (Kar04)	-16.88	2.5	0.60	50	0.03	Sw02a	Sw99	Sw02b/R	0.67±0.07	10
9179	5585	SAB(s)d	5.7 (Kar04)	-17.73	2.9	0.65	54	0.04	Cot91	Cot91	Cot91/R	1.07±0.05	8.8
9219	5608	Im/dS	10.2 (Jam04)	-16.35	1.3	0.51	59	0.03			Jan00/R	0.69±0.23	3.7
9248	5622	Sb	54.9	-20.11	0.9	0.58	55	0.06			Cou96/R	2.79±0.01	11
9465	5727	SABdm/LSB	26.4 (Jam04)	-18.25	1.1	0.52	73	0.04			Her96/I	2.29±0.01	12
9866	5949	SA(r)bc	7.4 (Jam04)	-17.07	1.1	0.47	57	0.06			Cou96/R	0.54±0.27	1.6
10075	6015	SA(s)cd	14.7 (Jam04)	-19.78	2.7	0.40	65	0.03			Her96/I	2.49±0.01	12
10310		SB(s)m	12.7 (Jam04)	-17.00	1.4	0.79	34	0.03	Sw02a	Sw99	VZ00/B	1.50±0.03	7.4
11557		SAB(s)dm	19.7 (Jam04)	-19.12	1.1	0.80	30	0.63	Sw02a	Sw99	Sw02b/R	1.70±0.02	8.6
11707		SAdm/LSB	15.9 (Sw02)	-17.54	1.8	0.52	55	0.44	Sw02a	Sw99	Sw02b/R	3.04±0.01	15
11914	7217	SA(r)ab	15.0 (Koo06)	-20.35	1.9	0.83	28	0.24	VM95	VM95	VM95/R	1.76±0.20	9.1
12060		IBm/LSB	15.7 (Sw02)	-16.60	0.8	0.65	40	0.24	Sw02a	Sw99	Sw02b/R	1.58±0.01	12

(1) name of the galaxy in the UGC catalog. (2) name in the NGC catalog when available. (3) morphological type from the RC3 catalog, completed by a mention LSB and dS as explained in section 2 of the text. (4) Distance and source. When no reference is given, the distance has been computed as explained in section 2 of the text. Jam04=James et al. 2004 ; Kar04=Karachentsev et al. 2004 ; Koo06=Koopmann et al. 2006 ; Mou06=Moustakas & Kennicutt 2006 ; Saha06=Saha et al. 2006 ; Sha01=Shapley et al.2001 ; Sw02=Swaters & Balcells 2002. (5) Absolute B magnitude computed from the corrected apparent B magnitude  $B_{T0}$  from the RC3 using the distance of column 4. (6) radius at 25 B mag/arcsec<sup>2</sup> from the RC3. (7) axis ratio at 25 B mag/arcsec<sup>2</sup> from the RC3.(8) inclination adopted for deriving the rotation curve. (9) Galactic absorption in the R band, computed as explained in section 2 of the text. (10) source of total HI distribution. Bro94=Broeils & van Woerden 1994 ; Cot91=Coté et al. 1991 ; Mo98= Moore 1998 ; Sw02a=Swaters & Balcells 2002 ; Ver01=Verheijen and Sancisi 2001 ; VM95=Verdes-Montenegro et al. 1995 ; War88=Warmels 1988 (11) source of HI rotation curve. Cot91=Coté et al. 1991 ; Mo98= Moore 1998 ; S02=Stil 2002 ; Sw99=Swaters 1999 ; vD94=van Driel 1994 ; Ver01=Verheijen & Sancisi 2001 (12) source of photometry and corresponding band. Cot91=Coté et al. 1991 ; Cou96=Courteau 1996 ; Dej94=De Jong 1994 ; Her96=Héraudeau and Simien 1996 ; Jan00=Jansen et al.2000 ; Kas06=Kassin et al.2006b ; OHP120=Observed by Spano with 1.20m OHP in March 2006 ; Sw02b=Swaters et al. 2002 ; vD94=van Driel 1994 ; VZ00=van Zee 2000 (13) Disk scale length, in kpc, derived from the photometric profile of column 12, with distance of column 4. (14) Radius of the last point, in kpc, of the rotation curve.

these classes. Our whole sample is in fact not big enough to reach strong conclusions and most results presented here are trends to be confirmed.

When HI data were available (which is the case for more than half of the selected sample) we derived an hybrid rotation curve, by combining our optical data with the HI data from the literature. Table 1 gives the origin of the HI data

(when available) and of the photometry data used to derive our mass models. The morphological types are also given in that table, together with the main parameters adopted for the galaxies analyzed in this paper (distance, radius at 25 B mag/arcsec<sup>2</sup>, axis ratio and Galactic absorption).

The distances for each galaxy are also given together with the corresponding references in the literature. Some

of these distances are based on local indicators such as the brightest supergiants, cepheids, red giant branch position or group membership but most of them are based on the Hubble law, assuming  $H_o=75 \text{ km s}^{-1} \text{ Mpc}^{-1}$  and taking into account the Virgo Infall. When no precise value of distance was found in the literature, we simply divided by  $H_o=75 \text{ km s}^{-1} \text{ Mpc}^{-1}$ , using the velocity correction for infall of the Local Group towards Virgo (vvir) given in the HyperLeda data base.

The galactic absorption in the R band has been determined from that in the B band given in the HyperLeda data base, assuming  $A(R)/A(B)=0.62$  (from the values of  $A(R)/A(V)$  and  $A(B)/A(V)$  given in Table 6 of Schlegel et al. 1998, evaluated using the  $R_V=3.1$  extinction laws of Cardelli et al. 1989 and O'Donnell 1994). The value  $A(R)/A(B)=0.62$  has been confirmed by Choloniewski & Valentijn 2003 using a new method for the determination of the extinction in our Galaxy, based on the observation of surface brightnesses of external galaxies in the B and R bands. Only 4 galaxies of our sample are affected by a relatively strong Galactic absorption in the R band (between 0.4 and 0.6 (see column 8 of Table 1) which should not affect our conclusions.

### 3 THE DATA SET

#### 3.1 The hybrid rotation curve

The hybrid rotation curve was obtained with the following method.

In the central part of the galaxy, we preferred the  $H\alpha$  curve because of its higher spatial resolution. The curve was extended in the outer parts with the HI data when available.

The rotation curves given on figures 6 to 14, in the annex, show the hybrid rotation curve used for the fit of the models, with full dots for the  $H\alpha$  velocities and open circles for the HI velocities. The HI data in the inner parts are displayed as crosses, for comparison with our  $H\alpha$  data, but they are not used when fitting the models.

The  $H\alpha$  rotation curves of the GHASP survey are derived from the 2D velocity fields obtained from the scan of the  $H\alpha$  line with a Fabry-Perot. Each velocity field is composed of a lot of individual radial velocity points (hereafter mentioned as velocity pixels) since a velocity is computed for each pixel as soon as the signal to noise ratio is sufficient. The error bars of our rotation curves were computed up to now, for every point of the curve, from the velocity dispersion found among the velocity pixels contributing to that very point. Each galaxy being considered as a rotating disk, the velocity pixels contributing to a given point of the rotation curve are found to be lying within an elliptical ring in the sky. However, we do not take into account the points too close from the minor axis (otherwise the dispersion increases rapidly because the non circular motions are then amplified when converting radial velocities into rotational velocities). Also, when computing the final rotation curve, both approaching and receding sides are averaged.

The velocity points of the rotation curve resulting from the average of a large number of velocity pixels are much more accurate and reliable than those obtained from a limited number of pixels. That is why we weight the original

dispersion by the number of velocity pixels contributing to a given point of the rotation curve. To do that, we simply divide the original error bar by the square root of this number.

Whenever a rotation velocity point is computed from a too small number of velocity pixels we simply attribute to this point the average error bar found for the other points of the rotation curve.

The inclination adopted for deriving the rotation curves from the radial velocities (given in Table 1) are generally close from the values found in the literature and deduced from the photometric axis ratio (also given in Table 1). However, in some cases we found a significantly smaller dispersion of the rotation velocities when adopting a different inclination. Note also that the inclination has been changed for two GHASP galaxies previously published in Garrido et al. 2005: for UGC 11557 it is now  $30^\circ$  instead of  $37^\circ$  and for UGC 11914 it is now  $28^\circ$  instead of  $35^\circ$ . The highest rotation velocity dispersions are found for the smallest inclinations since the original radial velocities are then divided by the sine of the inclination, leading to large error bars on the rotation curves of almost face-on galaxies. This effect remains marginal for inclinations between  $40^\circ$  and  $30^\circ$  (five galaxies of our sample are concerned) but becomes noticeable for inclinations smaller than  $30^\circ$  because it more than doubles any velocity fluctuation. Only three galaxies of our sample have such small inclinations: UGC 11914 at  $28^\circ$ , UGC 4456 at  $27^\circ$  and, the closest to face-on, UGC 2034 at  $19^\circ$ . Note that it is one of the three irregular galaxies excluded from the fits in Fig.2 to Fig.5 because of chaotic behavior and large error bars of the rotation curve.

Most of the galaxies of our sample are rather nearby. However, 6 of them have distances larger than 30 Mpc. They are of Sb, Sbc or Sc type and large enough on the sky so that there is no problem of sampling or spatial resolution for deriving their rotation curve. Indeed these 6 galaxies exhibit well behaved rotation curves with rather small error bars.

We defined a "quality parameter" for each rotation curve, going from 1 (for best quality curves) to 4 (for very low quality curves). This parameter was estimated from characteristics such as asymmetry, velocity dispersion, bar, etc. Surprisingly, no significant difference was found on our plots between low and high quality points (indeed the dispersion was about the same, whatever the quality parameter) and we finally decided not to use this parameter for the plots. Nevertheless, it is worth being mentioned that 12 galaxies of our sample have good quality RC (class 1): UGC 3876, 4499, 5175, 5721, 6778, 7323, 7524, 8490, 9866, 11557, 11707, 11914; 11 galaxies have acceptable quality RC (class 2): UGC 4256, 4456, 4555, 5279, 7876, 9179, 9219, 9248, 9465, 10075, 12060; 9 galaxies have low quality RC (class 3): UGC 2034, 2455, 2503, 4325, 5272, 5842, 7045, 7901, 10310; 4 galaxies have very low quality RC (class 4): UGC 4274, 5789, 6537, 7699.

#### 3.2 The luminosity profile

We used the photometric data in the R band from the literature in order to derive the distribution of stellar mass. Additionally 4 galaxies were observed in March 2006, with the 1.20m telescope at OHP, in order to get their luminosity profile in the R band (see Table 1 for details). For UGC 9465

and UGC 10075 only the I band was available in the literature and we used the color indexes to derive the R band. For this purpose we used the effective color indexes V-I and I-R given by Prugniel & Héraudeau 1998 as a function of the morphological type of galaxies. Same thing for UGC10310 for which only the B band was found in the literature, we derived the R band now using B-V and V-R from Prugniel & Héraudeau 1998. An exponential was then fitted to the outer parts of the photometric profile and subtracted in order to check for the presence of a central bulge. Whenever a bulge was seen on the residual luminosity profile we decomposed the profile into two components. However, some of these residuals were found to be a mere nucleus and not kept into account. Also, we assumed that galaxies later than Scd type had no bulge and discarded any central component for these galaxies. As a result, only 4 galaxies of our sample were decomposed into bulge and disk components (see Table 2). Best fit models for extracting the disk and bulge components were carried out by minimizing the  $\chi^2$  using the Minuit package, with the Simplex and Milgrad routines from Fletcher 1970.

The bulge component has been extracted from the observed luminosity profile in the central part of the galaxy, after extrapolating the exponential profile of the underlying disk by an exponential law :

$$\mu_{disk}(r) = \mu_o + 1.0857\left(\frac{r}{h}\right) \quad (1)$$

where  $\mu_o$  is the central surface brightness of the disk and  $h$  the disk scale length.

The remaining luminosity profile has been fitted by a de Vaucouleurs law :

$$\mu_{bulge}(r) = \mu_e + 8.3268\left[\left(\frac{r}{r_e}\right)^{1/4} + \left(\frac{r}{r_t}\right)^4\right] \quad (2)$$

where  $\mu_e$  is the central surface brightness of the bulge and  $r_e$  the bulge scale factor.  $r_t$  is the truncation radius (limit beyond which the bulge is no more detected, taken here as the radius where the luminosity of the bulge reaches the magnitude  $30/\text{arcsec}^2$ ).

This bulge profile was then subtracted from the total luminosity profile observed in order to get the true disk component alone. It is this last component that was used for the mass modelling and not the pure exponential component given above (which was merely an intermediate step to get the bulge profile as best as possible). Some discrepancies with other authors must be mentioned however. For instance we found no bulge component for UGC 7045, whereas Baggett et al. 1998 found one. Conversely we found a bulge for UGC 7901 and 11914, while Kassin et al. 2006a considered the bulge as negligible for both of them (which is especially surprising for UGC 11914 since it is an Sab galaxy).

### 3.3 The distribution of neutral gas

The distribution of neutral hydrogen (found in the literature) has been multiplied by 1.33 in order to take into account helium. The thickness of the disk was calculated for each galaxy, depending on its type, with the formula given by Bottinelli et al. 1983.

Then, the halo contribution is deduced from the contribution of the different components to the final rotation curve we observe :

$$V_{rot}(r) = (V_{gaz}^2 + V_{disk}^2 + V_{bulge}^2 + V_{halo}^2)^{0.5} \quad (3)$$

For 14 galaxies of our sample there is no HI distribution in the literature (see Table 1). However, since the influence of the neutral gas is most often negligible in the central part of the rotation curves of galaxies, it should not change our conclusions about the shape of the dark matter halo in the center.

In order to check that, we have run our models for the 6 galaxies of our sample having a strong HI contribution and set the HI component at zero. The comparison of the results, with and without HI, shows that the change in both  $R_o$  and  $\rho_o$  ranges from 0% to 33%, with an average around 15%. The change in  $\chi^2$  is slightly smaller, with an average around 10%.

## 4 DENSITY PROFILES AND FITTING PROCEDURE

The method used in this paper to model the mass distribution is the same as described in Blais-Ouellette et al. 2001.

Since we have no a priori knowledge of the dark matter halo shape, we assumed the simplest shape of a spherical and symmetric distribution of matter (isothermal sphere):

$$\rho(r) = \frac{\rho_o}{\left(1 + \left(\frac{r}{R_o}\right)^2\right)^{3/2}} \quad (4)$$

where  $R_o$  is the core radius, and  $\rho_o$  the central density of dark matter. This kind of profile is flat in the center. However, N-body simulations, in the framework of the  $\Lambda$ CDM theory, favor cuspy halo profiles, peaked in the center (e.g. Navarro, Frenk & White, 1997, Moore et al. 1999, Fukushige & Makino 2001)

For instance, the NFW profile is :

$$\rho_{NFW}(r) = \frac{\rho_o}{\left(\frac{r}{R_o}\right)\left(1 + \frac{r}{R_o}\right)^2} \quad (5)$$

where  $R_o$  is the core radius and  $\rho_o$  is the central density of dark matter. The density  $\rho(r)$  is thus proportional to  $r^{-1}$  when  $r$  is small.

We used for our fits the density profiles defined by Zhao 1996 :

$$\rho(r) = \frac{\rho_o}{\left(c + \left(\frac{r}{R_o}\right)^{-\gamma}\right)\left(1 + \left(\frac{r}{R_o}\right)^\alpha\right)^{\frac{\beta+\gamma}{\alpha}}} \quad (6)$$

where  $\rho_o$  is the central density and  $R_o$  the core radius. The density profiles are then defined by the set of parameters  $(c, \alpha, \beta, \gamma)$ . Our fitting procedure was led with the two following sets : (0,2,3,0) corresponding to the isothermal sphere (equation 4) with a constant central density and (0,1,3,-1) corresponding to the NFW profile (equation 5), with a peaked central density.

For each of the 36 galaxies studied here, we have applied the best fit model technique for these two profiles (isothermal sphere, hereafter ISO, and NFW). It consists in minimizing the  $\chi^2$  in the 3 dimensions of the parameter space defined by  $((M/L)_{disk}, \rho_o, R_o)$ . Whenever a bulge component is taken into account, a 4th dimension is added with  $(M/L)_{bulge}$ .

Some constraints were added to these parameters in order to avoid non physical values. We thus limited M/L to a

minimum value of 0.1 for both disk and bulge,  $R_o$  to a minimum value of 1kpc and  $\rho_o$  to a minimum value of  $10^{-3}$  solar masses  $\text{pc}^{-3}$ . These minima values were arbitrarily chosen (although suggested by the current values encountered for these parameters).

Table 2 summarizes the results of the best fits obtained with our mass models (for both NFW and ISO profiles of the dark matter halo) in terms of luminosity ratios of the visible components, central density and core radius of the dark matter halo together with the corresponding  $\chi^2$ .

For the calculation of our mass luminosity ratios, we adopted 4.28 for the absolute magnitude of the sun in the R band (Allen Astrophysical Quantities, 4th edition, 2000).

Figures 6 to 14, given in the annex, show the plots of the best fits obtained using the two different density profiles for the dark matter halo (isothermal sphere and NFW) for the 36 rotation curves of our sample. The observed rotation curves are coded as explained in section 3.1. The dotted blue (light) line is for the HI component. The dashed-dotted blue line is for the disk component. The dashed-dotted pink line is for the bulge component. The dashed green line is for the halo component. The continuous red line is for the total (quadratic sum of all components).

## 5 RESULTS OF THE FITS

### 5.1 Best fit model

For 10 galaxies, the halo is clearly the dominating component at all radii, whatever the model (NFW or ISO). They are UGC 4274, 5279, 5721, 5789, 5842, 7699, 7876, 9219, 11707 and 12060. All of them are late type spirals (from Scd to Im).

For 10 galaxies, the halo is dominating except in the very center (where the disk - or bulge - is the main component) and for ISO model only. They are UGC 4256, 4499, 6537, 6778, 7524, 7901, 8490, 9179, 10075 and 11557 (types ranging from Sc to Sm).

For 4 galaxies the disk is dominating at all radii whatever the model. They are UGC 2503, 5175, 9248 and 9866. All of them being rather early type galaxies (Sb or Sbc).

For 2 galaxies the disk (or disk + bulge) is dominating in the center whatever the model. They are UGC 2455 and UGC 11914. The result is not so surprising for this last one (being of Sab type) and more surprising for UGC 2455 (of Im type) but it must be taken with care because both models (NFW and ISO) led to abnormally low (non physical) values of M/L for this galaxy (blocked at 0.1 adopted here as the lowest acceptable value).

For the 10 remaining galaxies, the main component changes with the model but the disk is almost always dominating with the ISO model whereas the halo is dominating with the NFW model (the only exception being UGC 4325, for which the main component is the halo with the ISO model and the disk with the NFW model). These galaxies are mainly UGC 2034, 3876, 4555, and 7045, ranging from Sbc type to Im. Things are not so clear for UGC 4456, 5272, 7323, 9465 and 10310 (one Sc and four magellanic galaxies) because the disk is then overtaken by the halo in the outer parts with the ISO model.

Following the above discussion, we defined a classification code given in the last column of Table 2. To summarize,

we find 10 galaxies in class 0, 10 in class 1, 4 in class 2, 2 in class 3 and 10 in class 4.

This quick review of the results of the best fits confirms the well known fact that later type galaxies are more dark matter dominated.

Some galaxies of our sample have already been observed by other authors and their rotation curves have been analyzed in terms of mass models :

Four galaxies have been already observed by de Blok & Bosma 2002 all of them being LSB type galaxies : UGC 4325, 5272, 5721, 7524. They also observed UGC 10310 but could not derive mass models (except a minimum disk one) because they had no surface photometry. Our results are in good agreement for UGC 4325 and 5272, since they find good fits with their pseudo-isothermal model and bad ones with the NFW model. We also agree for UGC 7524, where they find that both models give acceptable fits. As for UGC 5721, we also find that the isothermal sphere provides a good fit but the fit we obtain with the NFW model is not satisfying (we find a  $\chi^2$  which is more than twice that obtained with the isothermal sphere) whereas they find it almost as good.

UGC 7323 (a dwarf galaxy of Sdm type) has been already observed by van den Bosch & Swaters 2001 who concluded that "no meaningful fit can be obtained for this galaxy". Our fits do not look so bad however, even with the NFW model for which we had to push down to the minimum acceptable value of M/L for the disk (0.1). Our best fit (smaller  $\chi^2$ ) was obtained with the isothermal sphere model, with a quite normal set of parameters.

Six dwarf or LSB galaxies have been already observed and analyzed in terms of mass models by Swaters et al. 2003 : UGC 4325, 4499, 5721, 8490, 11557 and 11707. They find better results for four of them (UGC 4325, 4499, 8490 and 11557) with a pseudo-isothermal model rather than with NFW (in agreement with our results except for UGC4499 that we discuss below) but they have a reverse for UGC 5721 (which is in contradiction with de Blok & Bosma 2002 and with our results) as well as for UGC 11707. About UGC 5721, we must confess that our ISO model gives a better solution to the price of minimal accepted values for both M/L (0.1) and  $R_o$  (1 kpc) thus casting a doubt on the validity of the result hence to the comparison that can be done with the NFW model for this galaxy. As for UGC 11707, we have H $\alpha$  points on the rotation curve hovering significantly above the HI curve for radii going from 3 to 6 kpc (see Fig.14), exactly where the pseudo-isothermal sphere model from Swaters et al. is too low to fit correctly the observed curve (see their Fig.3). The difference between our H $\alpha$  curves may be explained by the smaller value of inclination we adopted for that galaxy ( $55^\circ$  instead of  $68^\circ$ ) but also because with Fabry-Perot observations we take into account data from a large part of the disk instead of getting points only along a slit. We agree with Swaters et al. who find that NFW overpredicts the inner slope of the rotation curve for UGC 4325 (also in agreement with de Blok & Bosma 2002, Fig. 8) and for UGC 8490 (as can be seen on their figure 3) but not for UGC 4499 where the slope of our H $\alpha$  rotation curve can be fitted correctly with our models (even slightly better with the NFW model although it is not very significant). Indeed, the inner slope of their rotation curve is not much different from the slope of the HI curve (plotted as crosses on our Fig.

**Table 2.** Results of the best fits of rotation curves with isothermal sphere and NFW models of halo profiles

N°	N°	M/L	M/L	$R_o$	$\rho_o$	$\chi^2$	M/L	M/L	$R_o$	$\rho_o$	$\chi^2$	Best	Class
UGC	NGC	Disk	Bulge	kpc	$10^{-3}M_{\odot}pc^{-3}$		Disk	Bulge	kpc	$10^{-3}M_{\odot}pc^{-3}$		model	
(1)	(2)	ISO	ISO	ISO	ISO	ISO	NFW	NFW	NFW	NFW	NFW	(13)	(14)
2034		1.9		184	1	0.97	0.83		10	1	0.90	Both	4
2455	1156	0.10		30	5	1.24	0.10		5.8	1	2.33	ISO	3
2503	1169	6.8	1.5	188	1	1.27	6.0	0.73	57	1	1.91	Both	2
3876		7.9		100	23	0.60	0.19		33	5	0.47	Both	4
4256		0.27		3.4	49	0.60	0.10		6.8	19	0.74	Both	1
4274		0.42		1.0	253	2.34	0.43		2.3	60	1.73	NFW	0
4325	2552	2.6		1.9	121	2.50	9.00		2.7	1	2.90	Both	4
4456		1.0		15	1	1.54	0.20		14	2	1.48	Both	1
4499		1.7		2.2	43	0.90	0.15		4.3	19	0.76	Both	4
4555	2649	8.1		100	5	5.23	0.21		20	14	3.07	NFW	4
5175	2977	5.3		2.0	200	2.16	6.4		3.8	54	4.52	ISO	2
5272		2.6		25	14	1.10	0.21		25	1	1.44	Both	4
5279	3026	0.10		3.2	95	1.23	0.85		35	3	2.78	ISO	0
5721	3274	0.10		1.0	408	1.58	0.10		2.6	84	3.57	ISO	0
5789	3319	0.10		7.4	11	3.20	0.10		35	1	5.04	ISO	0
5842	3346	0.10		1.7	251	1.58	0.23		5.0	43	2.52	ISO	0
6537	3726	0.21		4.7	8.0	7.04	0.10		16	12	15.57	ISO	1
6778	3893	0.10	2.2	2.8	282	2.04	0.25	0.47	5.8	95	2.59	ISO	1
7045	4062	5.4		12	10	2.77	0.74		5.2	75	1.90	NFW	4
7323	4242	1.5		7.7	12	1.99	0.10		20	3	2.58	ISO	4
7524	4395	0.77		3.4	24	1.10	0.40		19	2	1.70	Both	1
7699		0.10		2.7	29	0.69	0.10		15	2	1.82	ISO	0
7876	4635	0.45		1.6	239	0.87	0.10		9.3	18	2.41	ISO	0
7901	4651	0.84	2.5	5.8	48	4.47	0.10	1.2	4.0	179	4.01	Both	1
8490	5204	1.1		1.9	95	0.62	0.16		4.5	26	2.09	ISO	1
9179	5585	0.31		2.8	69	3.41	0.10		16	5	9.51	ISO	1
9219	5608	0.10		1.8	40	2.88	0.10		5.0	6	6.86	ISO	0
9248	5622	4.1		1.7	75	5.13	4.9		1.0	10	5.18	Both	2
9465	5727	3.6		13	10	1.32	0.10		61	1	1.63	ISO	4
9866	5949	3.5		1.0	426	1.01	4.1		12	10	1.41	ISO	2
10075	6015	5.6		2.8	182	2.96	11		11	16	2.82	Both	1
10310		2.1		4.8	10	1.71	0.74		14	3	1.72	Both	4
11557		0.22		5.0	18	1.53	0.10		37	1	2.16	ISO	1
11707		0.10		2.4	84	2.59	0.25		6.1	19	3.81	ISO	0
11914	7217	4.2	6.2	13	63	2.12	2.7	5.9	16	32	2.78	Both	3
12060		0.76		4.6	26	2.74	0.10		14	5	3.15	Both	0

(1) name of the galaxy in the UGC catalog. (2) name in the NGC catalog when available. (3) M/L of the disk in the R band for the isothermal sphere model. (4) M/L of the bulge in the R band for the isothermal sphere model. (5) Core radius of the dark matter halo for the isothermal sphere model. (6) Central density of the dark matter halo for the isothermal sphere model. (7)  $\chi^2$  for the isothermal sphere model. (8),(9),(10),(11),(12), same as columns (3) to (7) but now with NFW profile for the dark matter halo model. (13) Best model: ISO, NFW or Both. (14) Classification of the RC according to the following code : 0 when Halo is the main component whatever the model, 1 when Halo is the main component except in the very center (and for ISO only), 2 when Disk is the main component at all radii whatever the model, 3 when Disk (or Disk + Bulge) is dominating in the center whatever the model, 4 when the main component is changing with the model (ISO or NFW).

8) whereas our  $H\alpha$  curve is clearly above. This discrepancy is maybe due to the fact that the authors use slit spectroscopy to get the  $H\alpha$  rotation curve in the central part of the galaxy (we adopted here the same inclination of  $50^\circ$ ), although they note that it generally provides a steeper slope than the HI curve, this last one being biased by beam smearing. As for the three other galaxies (UGC 5721, 11557 and 11707) we do find that NFW overpredicts the inner slope, more or less strongly but systematically.

Six galaxies of our sample have been studied by Kassin et al. 2006b (UGC 5789, 6537, 6778, 7045, 7901 and 11914, of respective types Scd, Sc, Sc, Sc, Sc and Sab) with another approach since they decompose the rotation curves found in

the literature into baryonic and dark matter components (stellar mass profiles are created by applying color-M/L relations to near-infrared and optical photometry). As a consequence, no straightforward comparison could be done with our results. However it is interesting to note that Kassin et al. find that for two of them (UGC 5789 = NGC 3319 and UGC 7045 = NGC 4062) the baryons underpredict the rotation curve, although they conclude that the case is not so clear for NGC4062 when taking into account all the uncertainties. Indeed, for UGC 5789 our models (NFW and ISO) both point at an M/L ratio of the disk at the minimum accepted value, 0.1, suggesting that it is dominated by the dark matter halo component. As for UGC 7045, the disk

alone (with  $M/L = 5.4$ ) is almost sufficient to explain the rotation curve with the ISO model (which is then very close to a maximum disk model) whereas it is the contrary with the NFW model where the halo alone can explain the rotation curve ( $M/L$  is then found to be close to 1 for the disk). For the four other galaxies (UGC 6537, 6778, 7901 and 11914) we find that the fits obtained with the ISO model are not far from the fits provided by a maximum disk, more especially for UGC 6537 and 11914 where the match is perfect (we applied maximum disk models to the 36 galaxies studied in this paper but the resulting graphs are not presented here). Our analysis of the rotation curves in terms of mass models for these six galaxies is thus in good agreement with the conclusions reached by Kassin et al.

In summary, in the cases where some of our galaxies have already been modeled by other authors, the results tend to agree pretty well. In the few cases which differ, the reason for the discrepancy has most of the time been identified.

## 6 DISCUSSION

In order to allow a direct comparison, the  $\chi^2$  given in Table 2 have been computed using the same variation range for the parameters and the same step of calculus for both the ISO and the NFW mass models.

The comparison of the values of the  $\chi^2$  found for the best fits of both models clearly shows that the isothermal sphere profile for the dark matter halo gives better results than the NFW profile when fitting the observed rotation curves. In Fig.1 we plotted the minimum value of the  $\chi^2$  found with the ISO model as a function of that obtained with the NFW model for each galaxy. These last  $\chi^2$  are systematically larger. The column "best model" in Table 2 indicates which one, from ISO or NFW, gives the best results as can be judged from the fits displayed on Figures 6 to 14, with the mention "Both" when they give comparable results. It appears that there is a clear difference between ISO and NFW models as soon as there is a 20% difference in the corresponding  $\chi^2$ . It also confirms what the  $\chi^2$  values suggest, namely that the ISO model provides better fits than the NFW in most of the cases.

Indeed, the NFW model, because of its steep rise in the center, is often unable to fit correctly the observed rotation curve. Typical examples can be seen with UGC 5279, 5842, 7699, 7876, 9219, 9465 or 11557. For these galaxies (all of late type, ranging from Scd to Im) the central rising part of the rotation curves is completely missed by the NFW model, although the  $M/L$  ratio of the disk is most often pushed to its lowest acceptable value of 0.1 (except for UGC 5279 and UGC 5842 where it is found to be respectively 0.56 and 0.16).

In particular, in the case where the  $\chi^2$  value is lower for the NFW model, the  $M/L$  value found is smaller than for the ISO model, leading to a poor match between the RC and the disk contribution in the central region of the galaxy. More generally, because of the small  $M/L$  found for the NFW models, this solution rarely allows the first 1-2 kpc of the RC to be fitted by the disk component contribution, even when the shape of the RC should make it possible. Indeed, the ISO model solutions, which are often close to maximum disk solutions, lead to better matches between the stellar

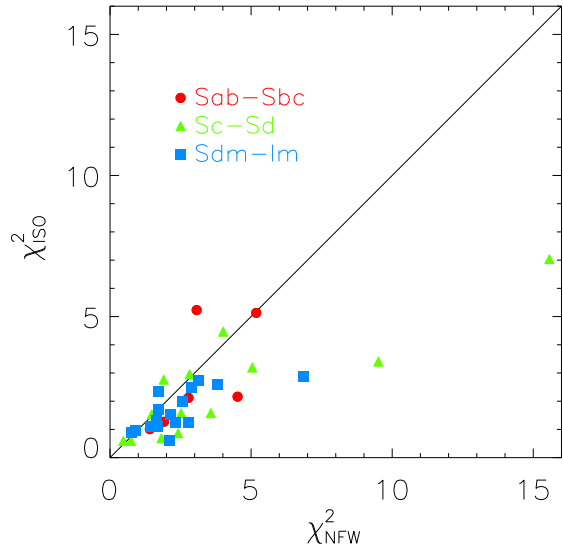


**Figure 1.** Minimum  $\chi^2$  obtained with an isothermal sphere profile versus a NFW profile. For figures 1 to 5 we used three different symbols for the main classes of morphological types of spiral galaxies (early, late and magellanic).

mass and the total mass distributions in the inner region of the galaxies. This is a strong argument in favor of the ISO solutions.

The NFW profile cannot account for rotation curves with a linear rise in velocity with radius, as shown by Hayashi & Navarro 2006 in their Fig.1. The ISO model, on the contrary, provides good fits in the central part for such slowly rising rotation curves and, more generally, systematically better fits than the NFW model for most of the galaxies of our sample. The position of the points on Fig. 1 shows no special trend with morphological type. More generally, it can be seen that the NFW best fits tend to give systematically unphysical low values for the disk  $M/L$  ratio (0.1). This is even a stronger argument than the smaller  $\chi^2$  to favor the ISO solutions. Also, whenever the  $\chi^2$  is smaller for the NFW model, it appears that the  $M/L$  is systematically smaller (or equal in one case) than with the ISO model, leading to abnormally low values of  $M/L$ .

Looking at Tables 1 and 2, one can see that nearly half (16/36) of the galaxies do not have HI velocities such that the RC is only defined in the inner parts. Since, as mentioned earlier, the kinematics in the inner parts can be affected by non-circular motions (such as the presence of bars), it is interesting to see if this alters significantly the results when trying to see which model (ISO or NFW) fits best the kinematics. In fact, for the whole sample (36) we get that 50% are best represented by an ISO model, 8% by an NFW model and 42% are equally well represented by both models while for the sub-sample having only an optical RC for the inner parts, those numbers are 50%, 12% and 38%. Thus, the main conclusions hold even when only optical data are available for the inner parts.

In Figure 2, we plotted the central density of the dark matter density profile versus the core radius of the dark halo for both models (top: isothermal sphere profile; bottom: NFW profile). The central density and the core radius of the halo are clearly correlated : the higher the central density, the smaller the core radius, whatever the model and independant of morphological type. This is in good agreement with the results found by other authors (Burket, 1995; Kravtsov et al. 1998 and Blais-Ouellette, 2000) who claim that one free parameter is enough for describing the distribution of dark matter. More recently, Barnes et al. 2004 and Kormendy & Freeman 2004 also found the same type of correlation. However, the slope of our correlation is close to that found by Kormendy & Freeman whereas the slope found by Barnes et al. is clearly steeper. Indeed, as detailed hereafter, we find a slope of -0.93 (for isothermal sphere fits) which is very close to that found by Kormendy & Freeman (-1.04 for isothermal sphere fits and -1.20 for pseudo-isothermal fits) while Barnes et al. find a steeper slope, around  $\sim -2$  (estimated from their Figure 4) for pseudo-isothermal sphere fits.

All these values are in agreement when considering the accuracy for the slopes. The error bars on our data show that the permitted range for the slope deduced from our Fig.2 (top) goes from 0.5 to 2.0. One can estimate this range from 1.5 to 2.5 for Barnes et al. and from 0.5 to 1.5 for Kormendy & Freeman.

When taking into account only the points for which the ISO model is clearly the best (see column 13 of Table 2) we also find a steeper slope (-1.38 instead of -0.93) intermediate between that found by Kormendy & Freeman and that found by Barnes et al. These points are surrounded by a circle on Figures 2 to 4. In figure 2 bottom (NFW model) these points also lead to a steeper slope than the whole set (-1.48 instead of -1.00). In figure 4 too, they suggest a slightly steeper slope (albeit the least-squares fit remains very flat and almost horizontal) than the whole set. In Figure 3 on the contrary, the points for which ISO is the best suggest a lower slope than the whole set for both graphs (top and bottom). For all these figures (2,3 and 4) these points tend to have a smaller dispersion than the whole set.

Based on published mass models for 37 galaxies, from Sc to Im type, Kormendy & Freeman found the following least-squares fit for isothermal halos:

$$\log \rho_o = -1.04 \log R_o - 1.02 \text{ (rms=0.17dex)}$$

Our data of Fig. 2 give the following least-squares fits excluding the 3 points plotted as open squares corresponding to Im galaxies discussed below about Figure 3):

$$\log \rho_o = -0.93 \log R_o - 0.74 \text{ (R}^2=0.61) \text{ for ISO}$$

$$\log \rho_o = -1.00 \log R_o - 1.03 \text{ (R}^2=0.42) \text{ for NFW}$$

We conclude that, on average,  $\log \rho_o \sim -\log R_o - 0.8$ , which implies that the product  $\rho_o R_o$  is almost constant.

Figure 3 shows the correlation of the central density (top) and of the core radius (bottom) as a function of absolute magnitude. From those two plots it is clear that faint galaxies (dwarfs) have higher central density and smaller core radius. In other words, dwarf galaxies have a more highly concentrated dark matter content than massive spirals. This result had already been seen quite convincingly in the study of the Sculptor group dwarfs by Côté et al. (2000) in their figures 8 and 9 (see also the figures 2 and 3 of Kormendy & Freeman 2004).

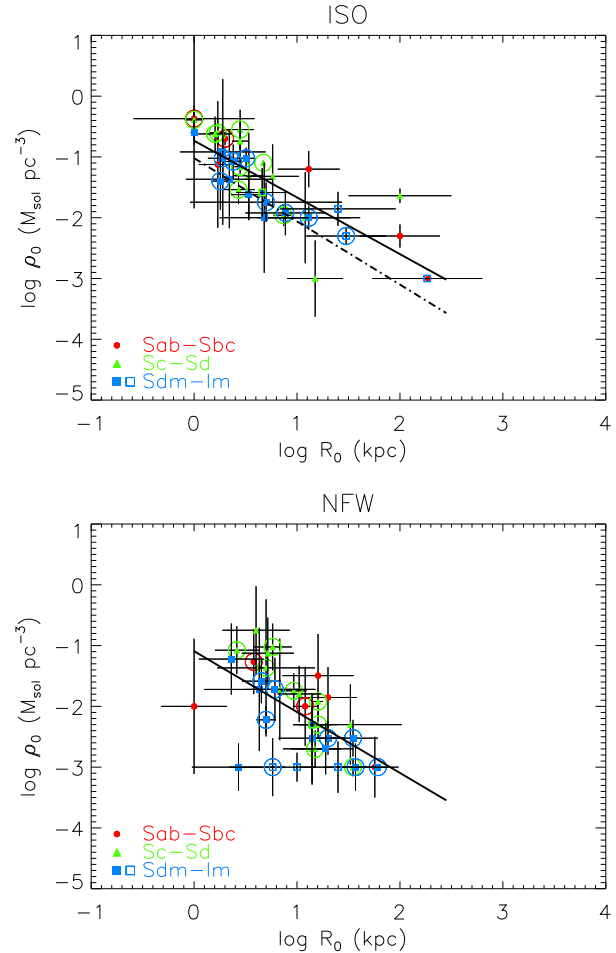


**Figure 2.** Top : Central density (log) of dark matter versus the core radius (log) of dark matter for the isothermal sphere profile (ISO). Bottom : Same for the NFW profile. The solid lines are least-squares fits to our data (excluding the 3 open squares discussed in section 6). The dashed line (top) is the least-squares fit extracted from figure 3 of Kormendy & Freeman 2004. Circles surround the points for which ISO is clearly the best model

For three out of the six Im galaxies of our sample (namely UGC2034, 2455 and 5272) the optical part of the rotation curve is very chaotic, with large error bars, and the resulting best fit models are not very reliable. The correlation is much clearer when these three galaxies are removed from the sample. Anyway we plotted them on the graphs as open squares but do not take them into account when fitting the data points. The same thing has been done for the two plots of Figure 2, where one can see that the corresponding points have a normal behavior on the top diagram (ISO model) whereas all of them appear in the lower part of the bottom diagram (NFW model) since they reach the minimum accepted value of  $\rho_o$ .

Kormendy & Freeman found the following least-squares fit for isothermal halos:

$$\log \rho_o = 0.113 M_B + 0.12 \text{ (rms=0.28dex)}$$

$$\log R_o = -0.127 M_B - 1.42 \text{ (rms=0.16dex)}$$

Our plots in Figure 3 give the following least-squares fits (also for the isothermal models):

$$\log \rho_o = 0.142 M_B + 1.29 \text{ (R}^2=0.12)$$

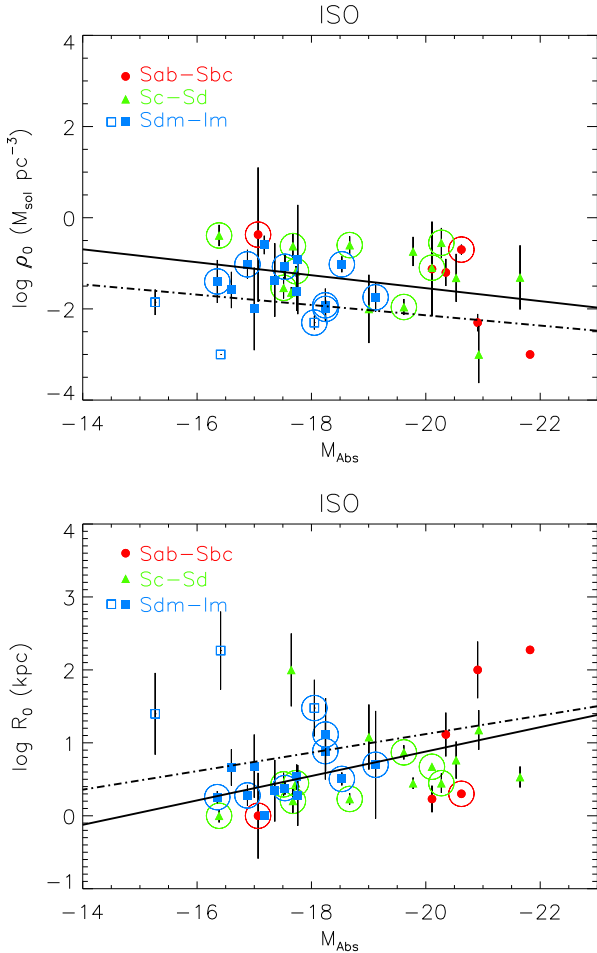


**Figure 3.** Top : Central density (log) of dark halo versus absolute magnitude. Bottom : Core radius (log) of dark halo versus absolute magnitude. Both are for the ISO models. The solid lines are least-squares fits for our data (excluding the 3 open squares discussed in section 6). The dashed lines are the least-squares fits extracted from figure 3 of Kormendy & Freeman 2004. Circles surround the points for which ISO is clearly the best model

$$\log R_o = -0.167 M_B - 2.47 \quad (R^2=0.23)$$

The agreement is fairly good, as can be seen on Figure 3, and strengthens the validity of these scaling laws.

Salucci et al. 2007 also get such a relation between the central density and the core radius of the halo (see Figure 1 of their paper) although for a different fitting model.

The obvious next step is to look at the product of  $R_o$  and  $\rho_o$  as a function of absolute magnitude. This is done in Figure 4. Our mass models, applied to galaxies ranging from Sab to Im, suggest a nearly constant halo surface density around  $\sim 150 M_\odot \text{pc}^{-2}$ , slightly higher than the value found by Kormendy & Freeman which is just below  $\sim 100 M_\odot \text{pc}^{-2}$  (according to their Fig. 5). Clearly, the halo surface density is nearly independent of galaxy luminosity. A small part of the offset ( $\sim 0.06$  for the log) observed on Figure 4 between our least-squares fit and that of Kormendy & Freeman may be explained by the adopted value of  $H_o=75 \text{ km s}^{-1} \text{ Mpc}^{-1}$  whereas they use  $H_o=70 \text{ km s}^{-1} \text{ Mpc}^{-1}$ , anyway the offset is smaller than the error-bars.

Another interesting correlation is the one found by Do-

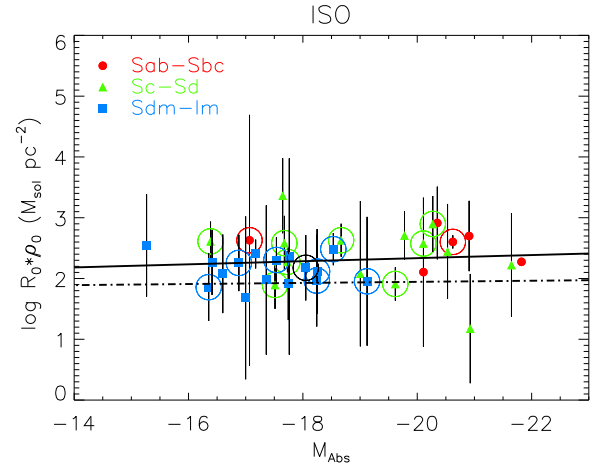


**Figure 4.** Central surface density (log) of dark matter (ISO model) as a function of absolute magnitude (given in Table 1, determined from  $B_T(0)$  found in the RC3 and our adopted distance). The solid line is a least-squares fit for our data (excluding the 3 open squares discussed in section 6). The dashed line is the least-squares fit extracted from figure 5 of Kormendy & Freeman 2004. Circles surround the points for which ISO is clearly the best model

nato et al. 2004 between the core radius of the dark matter halo and the exponential disk scale length  $h$ . They find (from a sample of 25 galaxies of different morphological types found in the literature) the following relation :

$$\log R_o = (1.05 \pm 0.11) \log h + (0.33 \pm 0.04)$$

$$\text{corr}=0.90 \quad \text{rms}=0.16 \text{dex}$$

Our data are in good agreement with that result since our plot of Figure 5 (top) shows the following relation (least-squares fit excluding the three Im galaxies already mentioned above and plotted as open squares) :

$$\log R_o = 0.996 \log h + 0.40 \quad (R^2=0.28)$$

The different types (LSB, dS, HSB) of galaxies are distinguished in Fig.5 (top) by circles of different sizes surrounding them (NB For those who are both LSB and dS we preferred marking only the last classification). Unfortunately 2 of the 5 dS of our sample are among the group of 3 galaxies already excluded from the fits in Fig.2 to 5 (where they are plotted as open squares). As a matter of fact, only 3 "bona fide" dS remain. Luckily, all of them are on the lower left side of the diagram, as expected, but of course it is not very significant and prevents to draw any significant conclusion.

Finally, as seen in Côté et al (2000), there is a trend in Figure 5 (bottom) between the core radius and the (B-V) color. The different types of galaxies are not distinguished in that figure because there are too few points to conclude efficiently about the different subtypes. Furthermore, it is just a trend that is shown, needing to be confirmed with a larger sample.

## 7 SUMMARY AND CONCLUSION

Our study, based on 36 galaxies of different morphological types, confirms the result already claimed by other authors about the shape of the dark matter halo in the center of spiral galaxies, namely that its density profile is probably

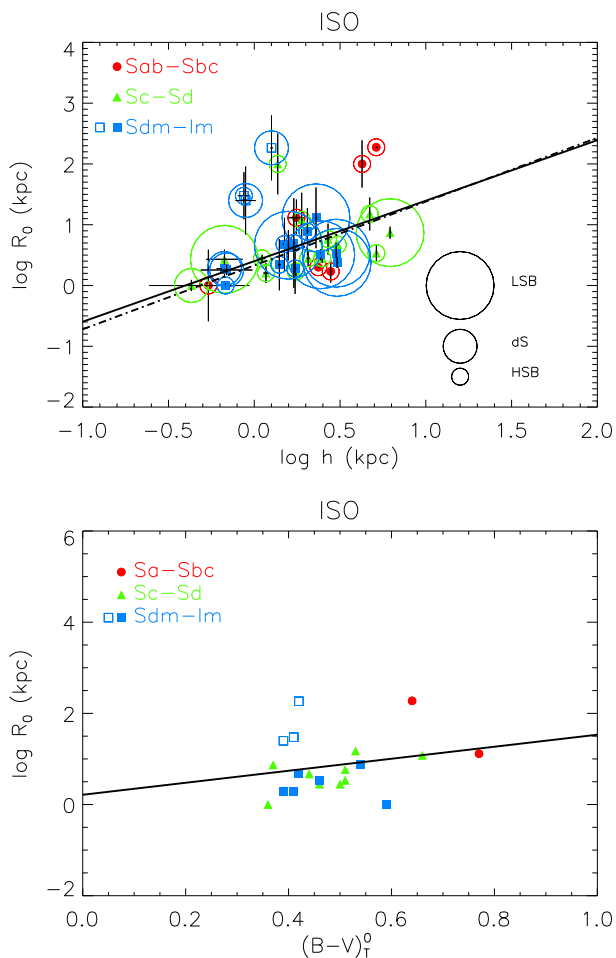


**Figure 5.** Core radius (log) of the dark matter halo (ISO models) as a function of optical disk scale length (top) and  $(B-V)$  color (bottom). This last parameter, extracted from the RC3 catalog, could be found for 20 of our galaxies only. The solid lines are least-squares fits obtained with our data (excluding the 3 open squares discussed in section 6). The dashed line on the top diagram is the least-squares fit from figure 1 of Donato et al. 2004. On that diagram we have surrounded HSB, dS and LSB galaxies by circles of growing sizes.

closer to an isothermal sphere profile than to an NFW profile: DM halos are rather flat than cuspy. Our mass models (ISO and NFW) are compared when fitting the rotation curve as a whole, however a comparison of the  $\chi^2$  values limited to the central regions would be still clearer since the inner slope of the RC found with the NFW model is systematically steeper and above the data points, compared with the ISO model.

Thus far, most of the results found in the literature concerned dwarf or Low Surface Brightness galaxies. 9 galaxies of our sample are LSB (UGC 2304, 5272, 5279, 5789, 7524, 7699, 9465, 11707 and 12060, with types going from Scd to Im) and, for all of them, we systematically find better results with the ISO model (smaller  $\chi^2$ ) than with NFW, except UGC 2304 for which both are equivalent. Interestingly, our study suggests that this holds for most spirals since the 36 galaxies of this study have morphological types ranging from Sab to Im. For almost all of them, the best fit is obtained

with the ISO model (the reverse is found only for 4 galaxies out of 36). Also, no significant difference can be seen when comparing the quality of the fits obtained with the NFW and the ISO model as a function of the morphological type.

However, a difference can be seen in the way the rotation curves are decomposed into several components, with the halo being the main component for late types and the disk (or disk + bulge) the main component for early types. This result, although needing to be confirmed with a larger sample, merely reflects the well known fact that later type galaxies are more dark matter dominated.

Finally, we confirm different halo scaling laws seen previously by other authors such as Côté et al (2000), Kormendy & Freeman 2004 and Barnes et al. 2004. Among those, it appears clearly that low luminosity galaxies have small core radius and high central density, the product of the two parameters being nearly constant with absolute magnitude. This means that the galaxy halo surface density is independent of galaxy type or luminosity. Trends are also seen for the core radius as a function of luminosity and color but should be confirmed with a larger sample.

## ACKNOWLEDGEMENTS

The authors wish to thank the anonymous referee who helped improve the paper. They thank the Groupement de Recherche Galaxies (now Programme National Galaxies) for its support for observing time and the Observatoire de Haute-Provence team for its technical assistance during the observations. They also thank O. Garrido, J.L. Gach, O. Boissin and P. Balard for their help during the observing runs and J. Boulesteix for constantly improving the ADHOCw software used for the data acquisition and reduction. The authors thank Chantal Balkowski, Laurent Chemin, Henri Plana and Olivier Daigle for fruitful discussions. This research has made use of the NASA/IPAC Extragalactic Database (NED) which is operated by the Jet Propulsion Laboratory, California Institute of Technology, under contract with the National Aeronautics and Space Administration. The authors have also made an extensive use of the LEDA database (<http://leda.univ-lyon1.fr>). CC and OH acknowledge support from the Natural Sciences and Engineering Research Council of Canada and le Fonds québécois de la recherche sur la nature et les technologies.

## REFERENCES

- Allen C. W. 2000, *Astrophysical Quantities*, 4th edition, Arthur N. Cox Editor.
- Baggett W. E., Baggett S. M., Anderson K. S. J. 1998, *AJ*, 116, 1626.
- Barnes E. I., Sellwood J. A., Kosowsky A. 2004, *AJ*, 128, 2724.
- Blais-Ouellette S., Carignan C., Amram P., Côté S., 1999, *AJ*, 118, 2123.
- Blais-Ouellette S., 2000, Ph.D. Thesis, Université de Montréal.
- Blais-Ouellette S., Amram P., Carignan C., 2001, *AJ*, 121, 1952.

- Blais-Ouellette S., Amram P., Carignan C., Swaters R., 2004, *A&A*, 420, 147.
- Bottinelli L., Gouguenheim L., Paturel G., de Vaucouleurs G., 1983, *A&A*, 118, 4.
- Broeils A.H. and van Woerden H., 1994, *A&AS*, 107, 129B.
- Burket A., 1995, *ApJ*, 447, L25.
- Cardelli J. A., Clayton G. C., Mathis J. S., 1989, *ApJ*, 345, 245.
- Choloniewski J., Valentijn E.A., 2003, *Acta Astron.* 53, 249.
- Coté S., Carignan C., Sancisi R., 1991, *AJ*, 102, 904.
- Coté S., Carignan C., Freeman K.C., 2000, *AJ*, 120, 3027.
- Courteau S. 1996, *ApJS*, 103, 363C.
- de Blok W.J.G., Bosma A., 2002, *A&A*, 385, 816.
- de Blok W.J.G., Bosma A., McGaugh S., 2003, *MNRAS*, 340, 657.
- de Jong R.S., van der Kruit P.C. 1994, *A&AS*, 106, 451D.
- de Jong, R.S., Bell, E. 2006, astro-ph/0604391. To appear in the conference proceedings of Island Universes, Structure and Evolution of Disk Galaxies, ed. R.S. de Jong (Springer, Dordrecht)
- Diemand J., Moore B., Stadel J., 2004, *MNRAS*, 353, 624.
- Donato F., Gentile G., Salucci P., 2004, *MNRAS*, 353, L17.
- Dutton A. A., Courteau S., de Jong R., Carignan C., 2005, *ApJ*, 619, 218.
- Epinat B., Amram P., Marcelin M., Balkowski C., Daigle O., 2008, *MNRAS*, to be submitted.
- Fletcher R., 1970, *Comp. J.*, 13, 317.
- Fukushige T., Makino J., 2001, *ApJ*, 557, 533.
- Garrido O., Marcelin M., Amram P., Balkowski C., Gach J.L., Boulesteix J., 2005, *MNRAS*, 362, 127.
- Garrido O., Marcelin M., Amram P., 2004a, *MNRAS*, 349, 225.
- Garrido O., Marcelin M., Amram P., Boissin O., 2003a, *A&A*, 399, 51.
- Garrido O., Marcelin M., Amram P., Boulesteix J., 2002, *A&A*, 387, 821.
- Graham A. W., Merritt D., Moore B., Diemand J., Terzic B., 2006, *AJ*, 132, 2701.
- Hayashi E., Navarro J. F., 2006, *MNRAS*, 373, 1117.
- Hayashi E., Navarro J. F., Springel, V., 2007, *MNRAS*, 377, 50.
- Héraudeau P., Simien F., 1996, *A&AS*, 118, 111.
- James P.A., Shane N.S., Beckman J.E., Cardwell A., Collins C.A., Etherton J., de Jong R.S., Fathi K., Knapen J.H., Peletier R.F., Percival S.M., Pollacco D.L., Seigar M.S., Stedman S., Steele I.A., 2004, *A&A*, 414, 23.
- Jansen R. A., Franx M., Fabricant D., Caldwell N., 2000, *ApJS*, 126, 271J.
- Karachentsev I.D., Karachentseva V.E., Huchtmeier W.K., Makarov D.I., 2004, *AJ*, 127, 2031.
- Kassin S.A., de Jong R.S., Pogge R.W., 2006a, *ApJS*, 162, 80.
- Kassin S.A., de Jong R.S., Weiner B.J., 2006b, *ApJ*, 643, 804.
- Koopmann R.A., Haynes M.P., Catinella B., 2006, *AJ*, 131, 716.
- Kormendy J., Freeman K.C. 2004, IAU Symposium 220. S. Ryder, D.J. Pisano, M. Walker & K.C. Freeman editors, p. 377
- Kravtsov A., Klypin A., Bullock J., Primack J., 1998, *ApJ*, 502, 48.
- Kuzio de Naray, R., McGaugh, S. S., de Blok, W. J. G., Bosma, A., 2006, *ApJS*, 165, 461
- Maccio A. V., Dutton A. A., van den Bosch F. C., Moore B., Potter D., Stadel, J., 2007, *MNRAS*, 378, 55.
- Moore B., Quinn T., Governato F., Stadel J., Lake G., 1999, *MNRAS*, 310, 1147.
- Moore E., Gottesman S., 1998, *MNRAS*, 294, 353.
- Moustakas J., Kennicutt R.C., 2006, *ApJS*, 164, 81.
- Navarro J., Frenk C., White S., 1997, *ApJ*, 490, 493.
- Navarro J., 2004, IAU Symposium 220. S. Ryder, D.J. Pisano, M. Walker & K.C. Freeman editors, p. 61
- O'Donnell J. E. 1994, *ApJ*, 422, 1580.
- Pizzella A., Corsini E.M., Dalla Bonta E.D., Sarzi M., Coccato L., Bertola F., 2005, *ApJ*, 631, 785.
- Prugniel P., Héraudeau P., 1998, *A&AS*, 128, 299.
- Saha A., Thim F., Tammann G.A., Reindl B., Sandage A., 2006 *ApJS*, 165, 108.
- Salucci P., Lapi A., Tonini C., Gentile G., Yegorova I., Klein U., 2007, *MNRAS*, 378, 41.
- Schlegel D. J., Finkbeiner D. P., Davis M. 1998, *ApJ*, 500, 525.
- Schombert J.M., Pildis R.A., Eder J.A., Oemler A., 1995, *AJ*, 110, 2067.
- Shapley A., Fabbiano G., Eskridge P. B., 2001, *ApJS*, 137, 139.
- Stil J., Israel F., 2002, *A&A*, 392, 473.
- Swaters R. A., Madore B. F., Trewhella M., 2000, *ApJ*, 531, L107.
- Swaters R. A., Madore B. F., van den Bosch F. C., Balcells M., 2003, *ApJ*, 583, 732.
- Swaters R.A., Balcells M., 2002, *A&A*, 390, 863.
- Swaters R.A., van Albada T.S., van der Hulst J.M., Sancisi R., 2002, *A&A*, 390, 829.
- Swaters R.A., 1999, Ph.D. thesis Rijksuniversiteit Groningen.
- van den Bosch, F. C., Robertson, B. E., Dalcanton, J. J., de Block, W. J. G., 2000, *AJ*, 119, 1579.
- van den Bosch F.C., Swaters R.A., 2001, *MNRAS*, 325, 1017.
- van Driel W., van Woerden H., 1994, *A&A*, 286, 395.
- van Zee L., 2000, *AJ*, 119, 2757.
- Verdes-Montenegro L., Bosma A., Athanassoula E., 1995, *A&A*, 300, 65.
- Verheijen M., Sancisi R., 2001, *A&A*, 370, 765.
- Warmels R.H., 1988, *A&AS*, 72, 427W.
- Zhao H., 1996, *MNRAS*, 278, 488.

## ANNEX

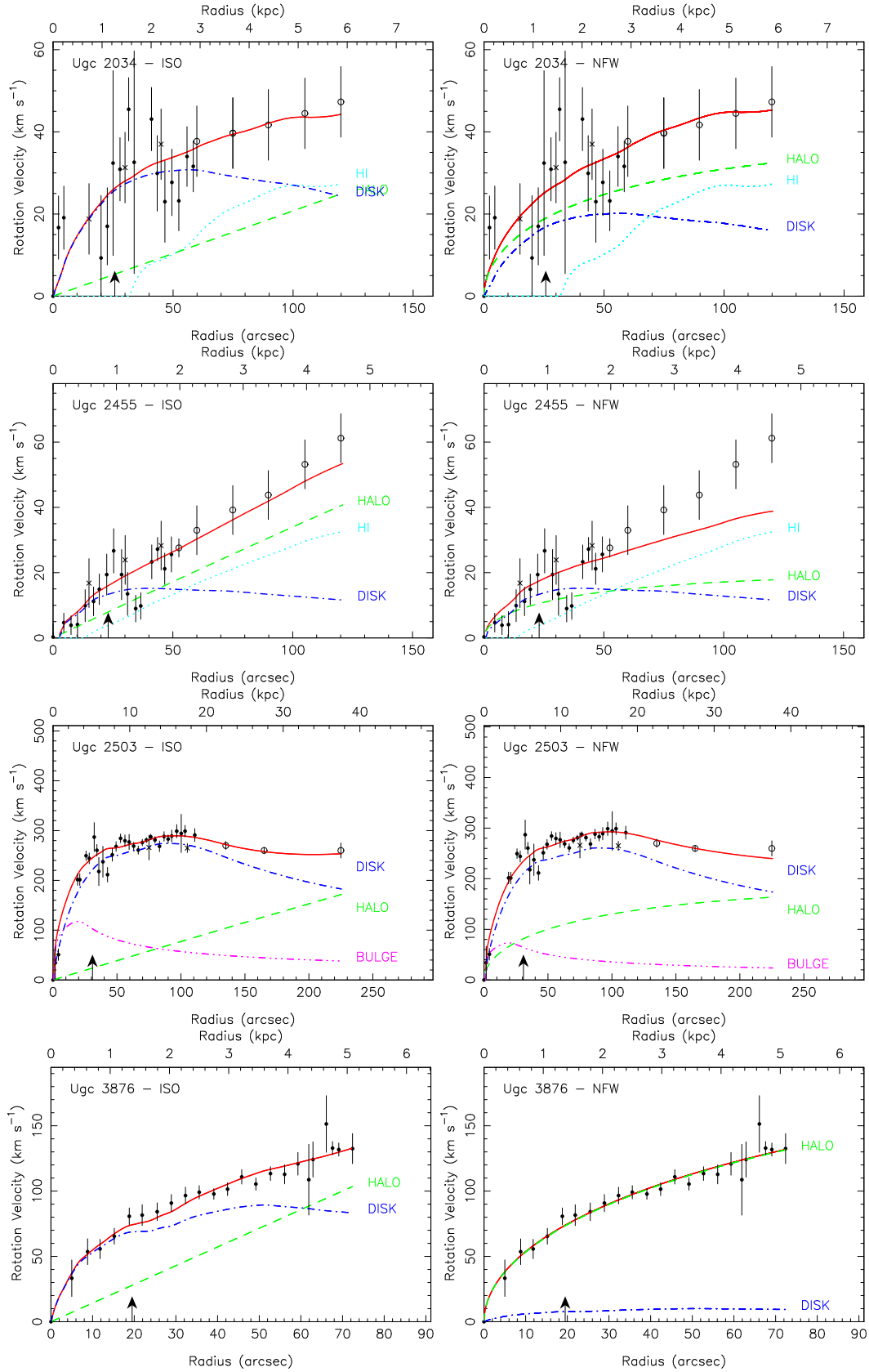


**Figure 6.** Best fit model for the rotation curve of UGC2034, UGC2455, UGC2503 and UGC3876 with isothermal sphere profile (left) and NFW profile (right). Dots are for optical velocities, open circles for HI velocities and crosses for HI in the central part, not taken into account. The arrow on the X axis indicates the disk scale-length.

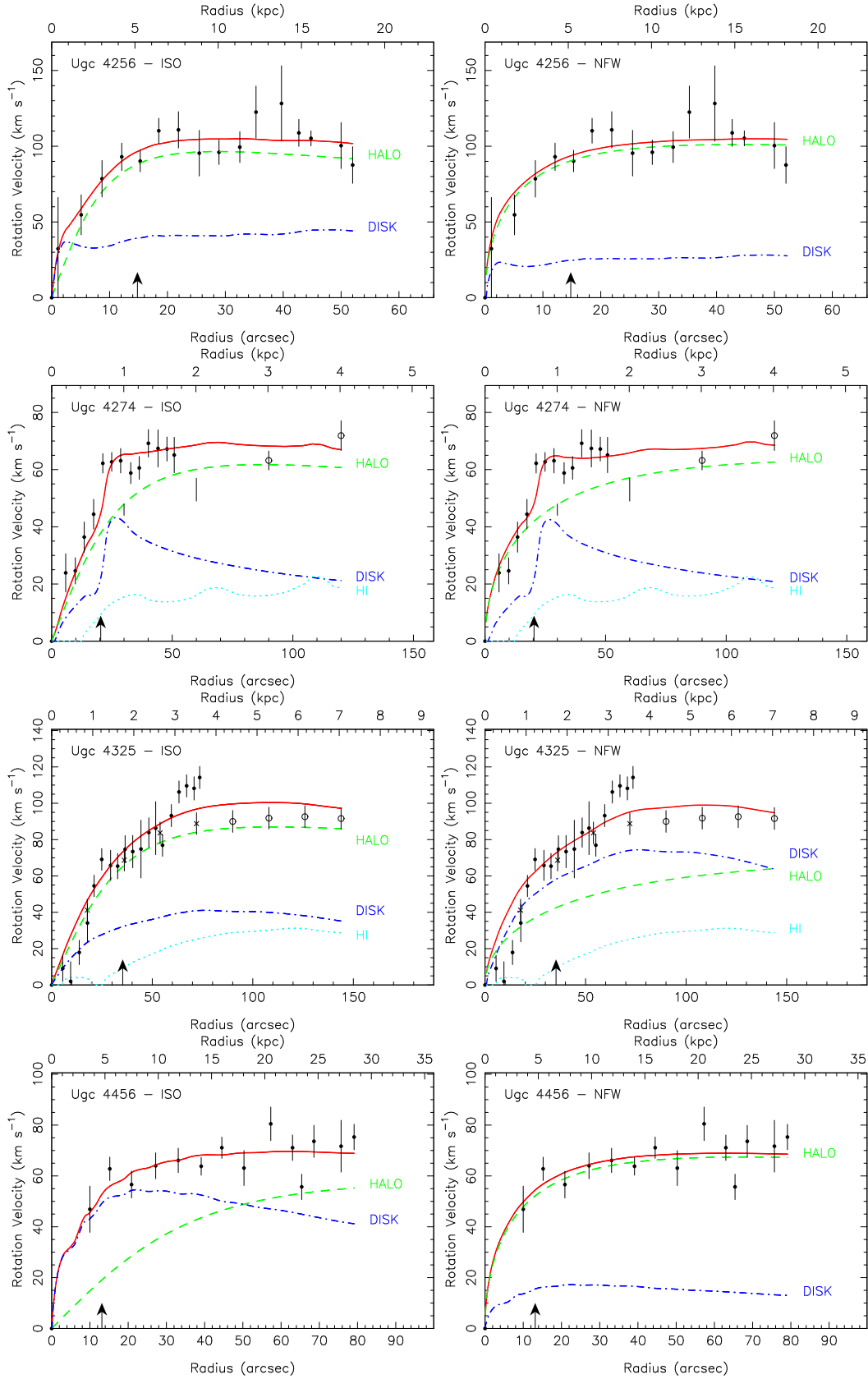


**Figure 7.** Best fit model for the rotation curve of UGC4256, UGC4274, UGC4325 and UGC4456 with isothermal sphere profile (left) and NFW profile (right). Dots are for optical velocities, open circles for HI velocities and crosses for HI in the central part, not taken into account. The arrow on the X axis indicates the disk scale-length.

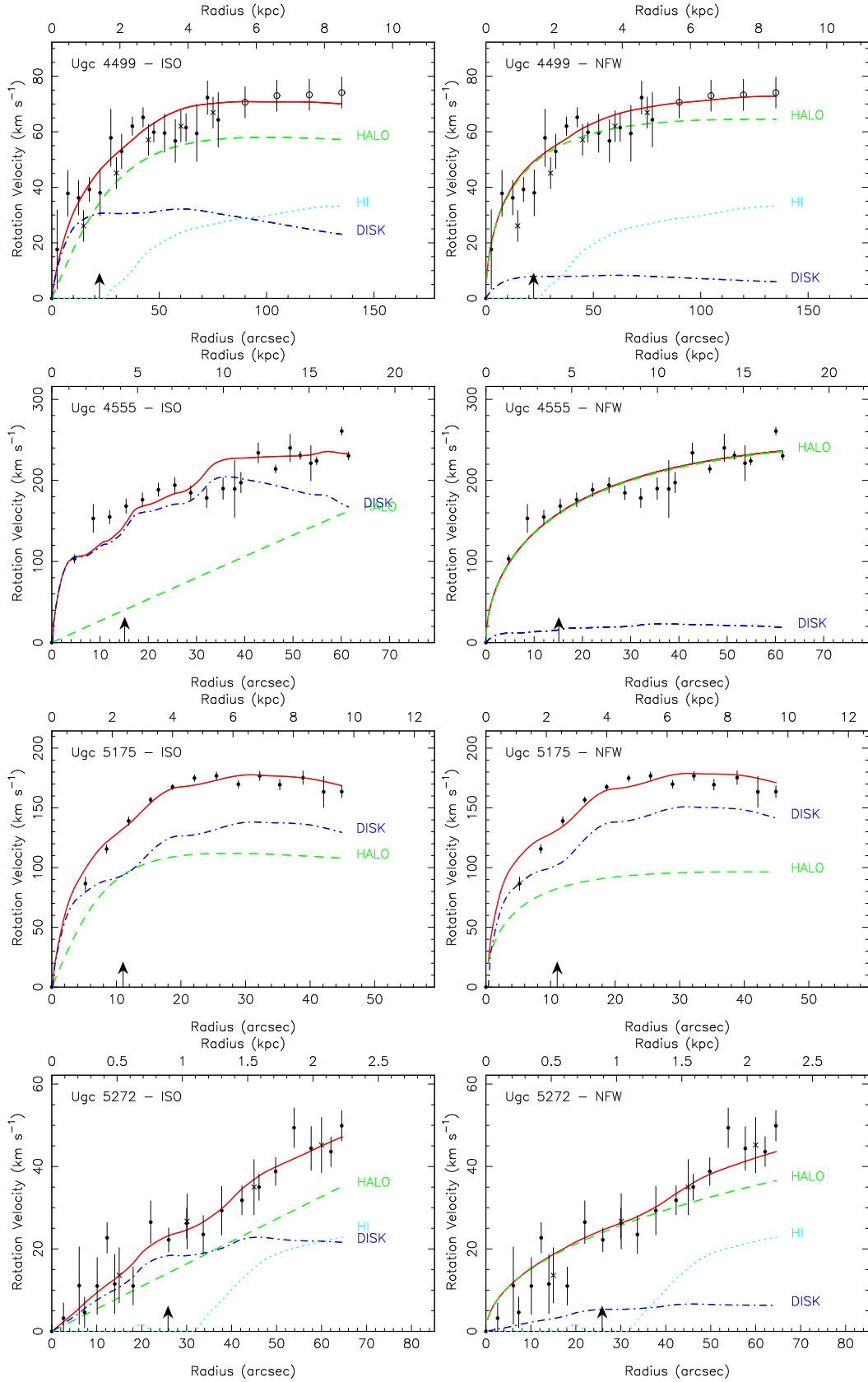


**Figure 8.** Best fit model for the rotation curve of UGC4499, UGC4555, UGC5175 and UGC5272 with isothermal sphere profile (left) and NFW profile (right). Dots are for optical velocities, open circles for HI velocities and crosses for HI in the central part, not taken into account. The arrow on the X axis indicates the disk scale-length.

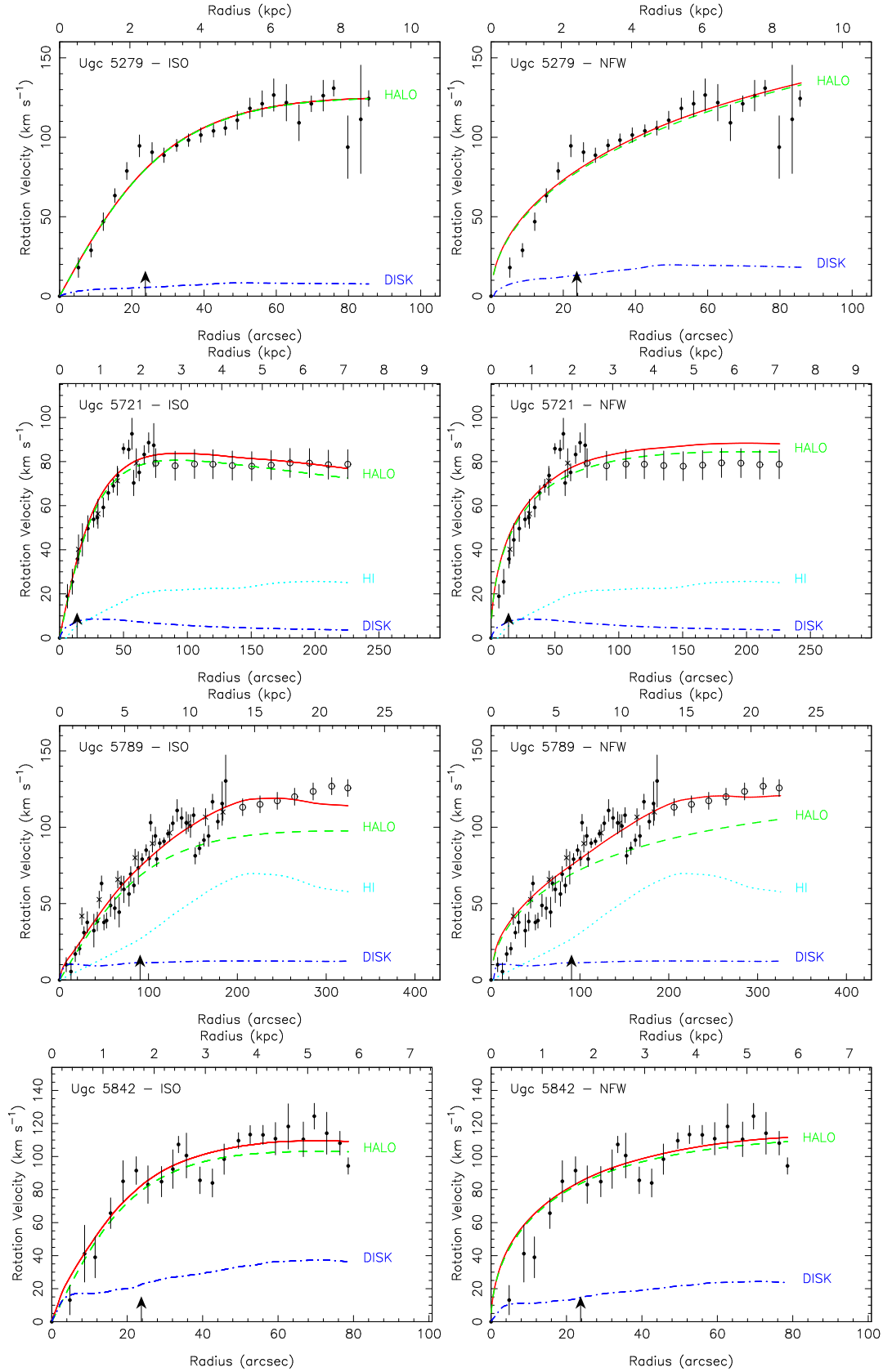


**Figure 9.** Best fit model for the rotation curve of UGC5279, UGC5721, UGC5789 and UGC5842 with isothermal sphere profile (left) and NFW profile (right). Dots are for optical velocities, open circles for HI velocities and crosses for HI in the central part, not taken into account. The arrow on the X axis indicates the disk scale-length.

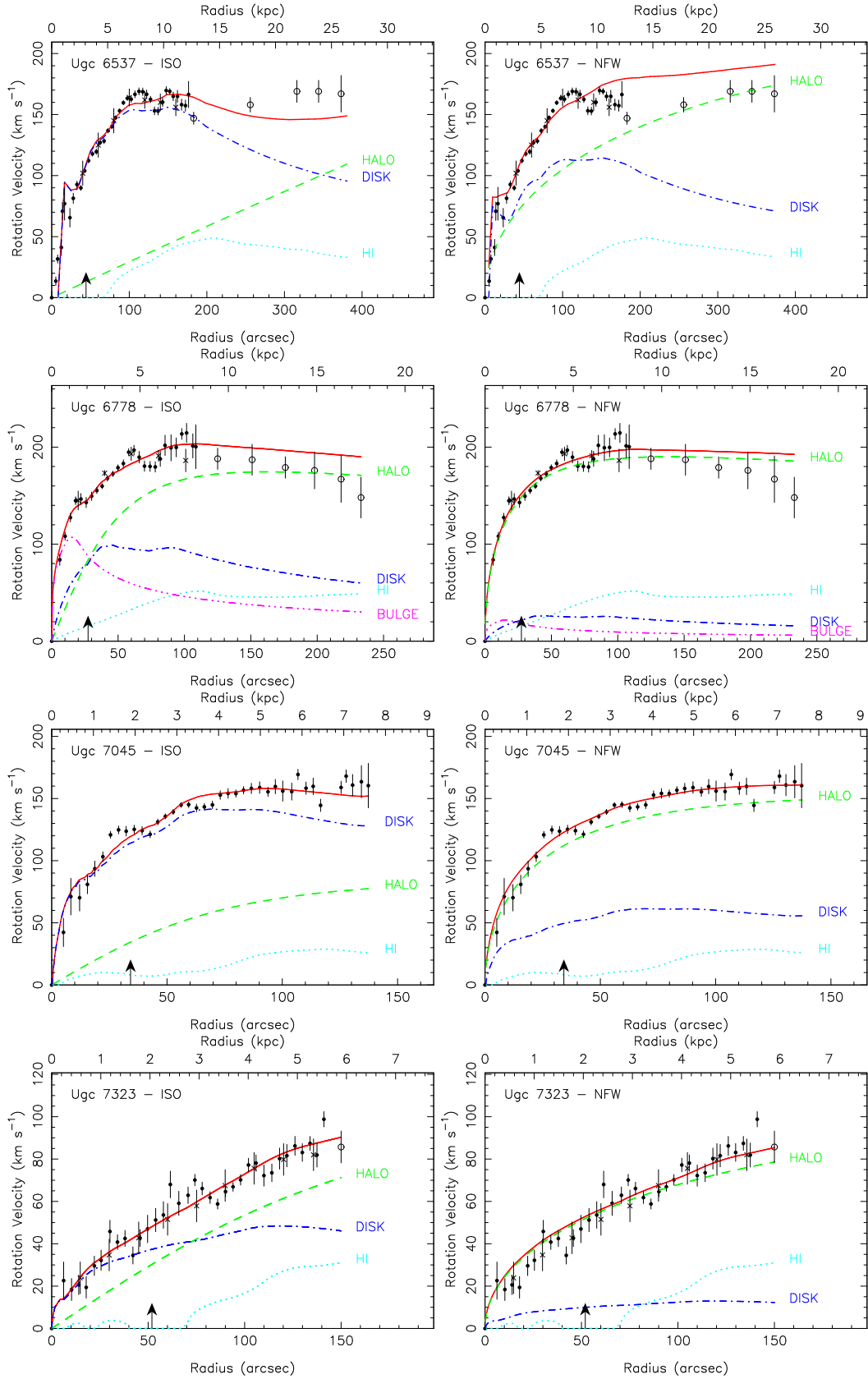


**Figure 10.** Best fit model for the rotation curve of UGC6537, UGC6778, UGC7045 and UGC7323 with isothermal sphere profile (left) and NFW profile (right). Dots are for optical velocities, open circles for HI velocities in the central part, not taken into account. The arrow on the X axis indicates the disk scale-length.

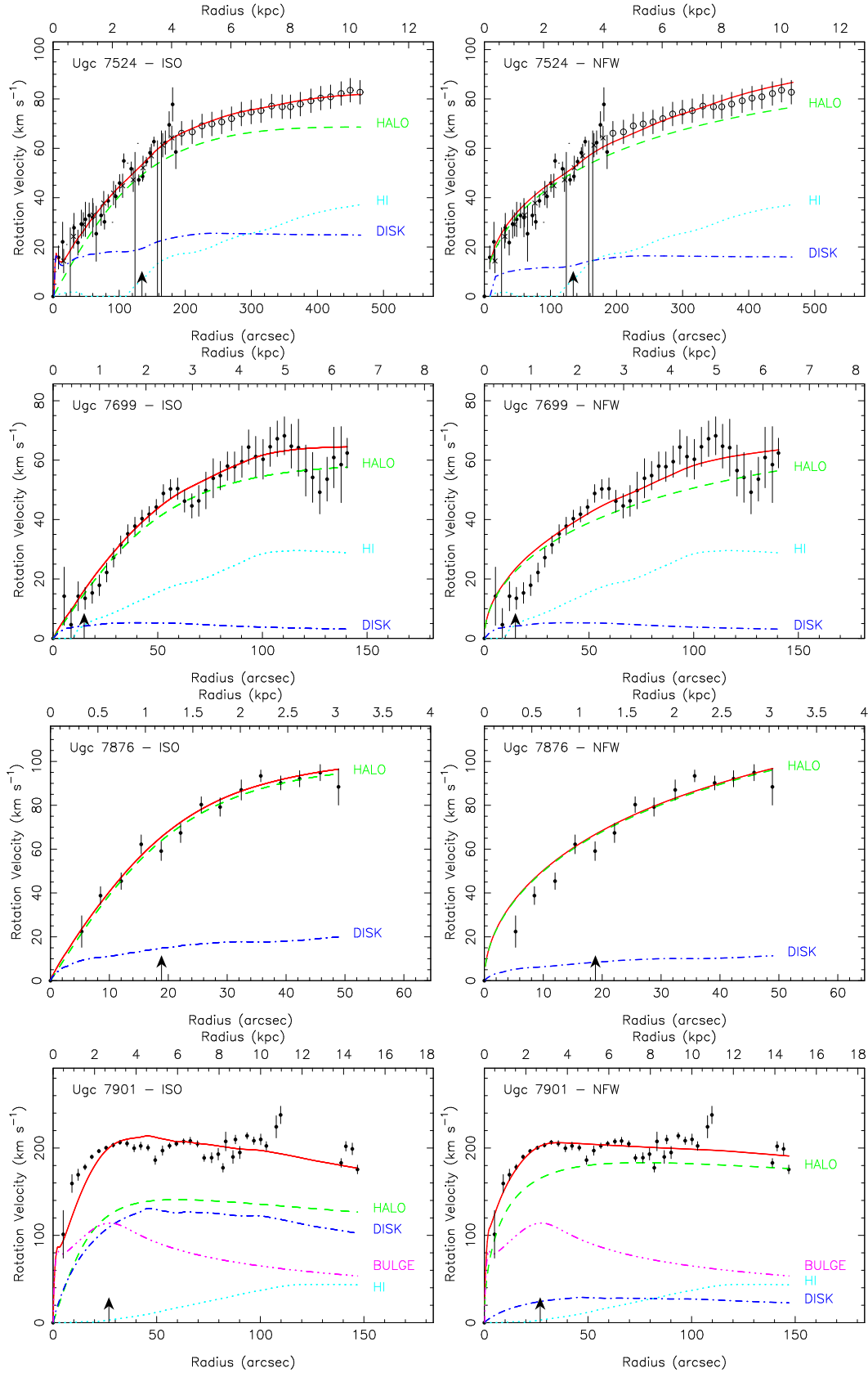


**Figure 11.** Best fit model for the rotation curve of UGC7524, UGC7699, UGC7876 and UGC7901 with isothermal sphere profile (left) and NFW profile (right). Dots are for optical velocities, open circles for HI velocities and crosses for HI in the central part, not taken into account. The arrow on the X axis indicates the disk scale-length.

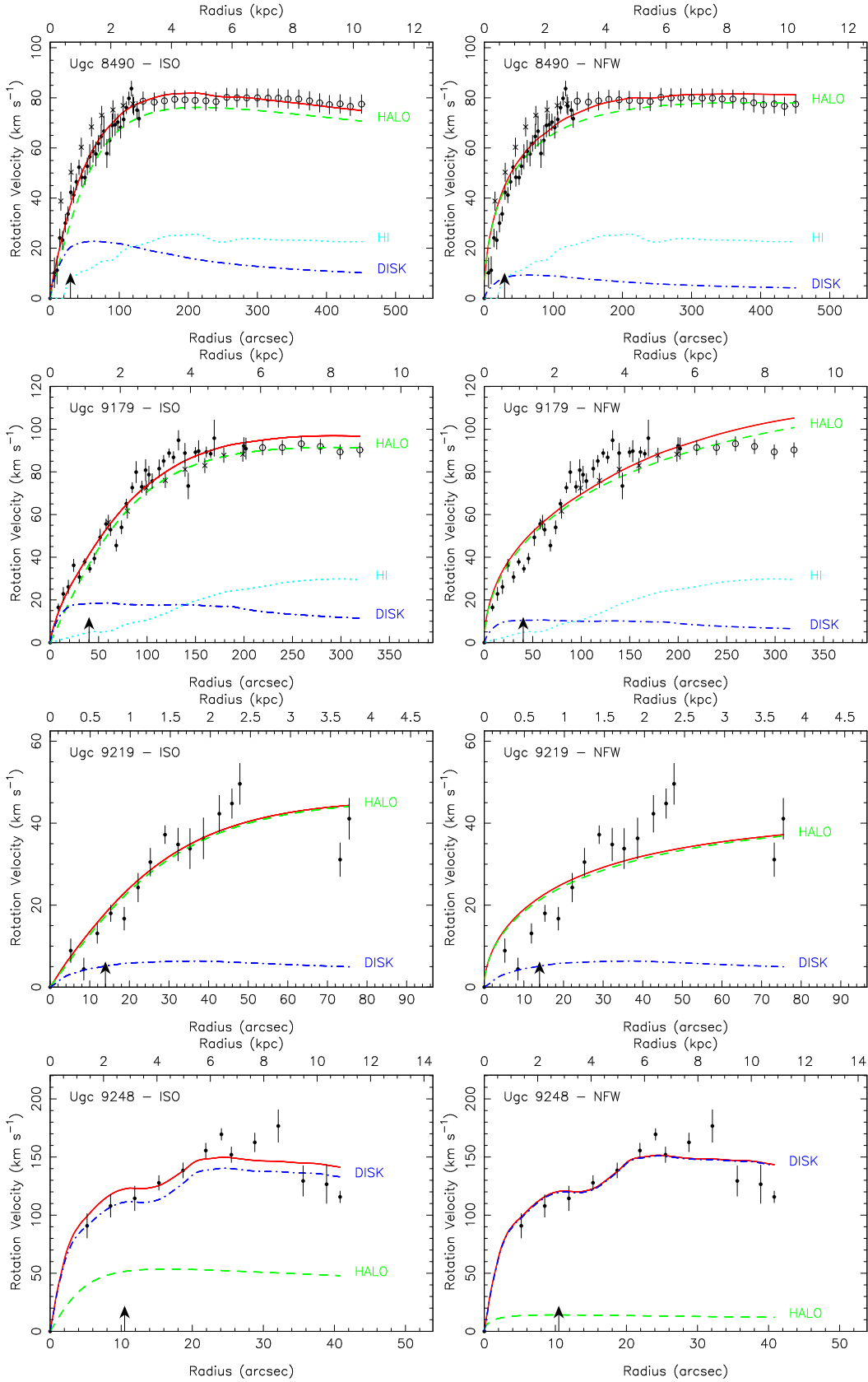


**Figure 12.** Best fit model for the rotation curve of UGC8490, UGC9179, UGC9219 and UGC9248 with isothermal sphere profile (left) and NFW profile (right). Dots are for optical velocities, open circles for HI velocities and crosses for HI in the central part, not taken into account. The arrow on the X axis indicates the disk scale-length.

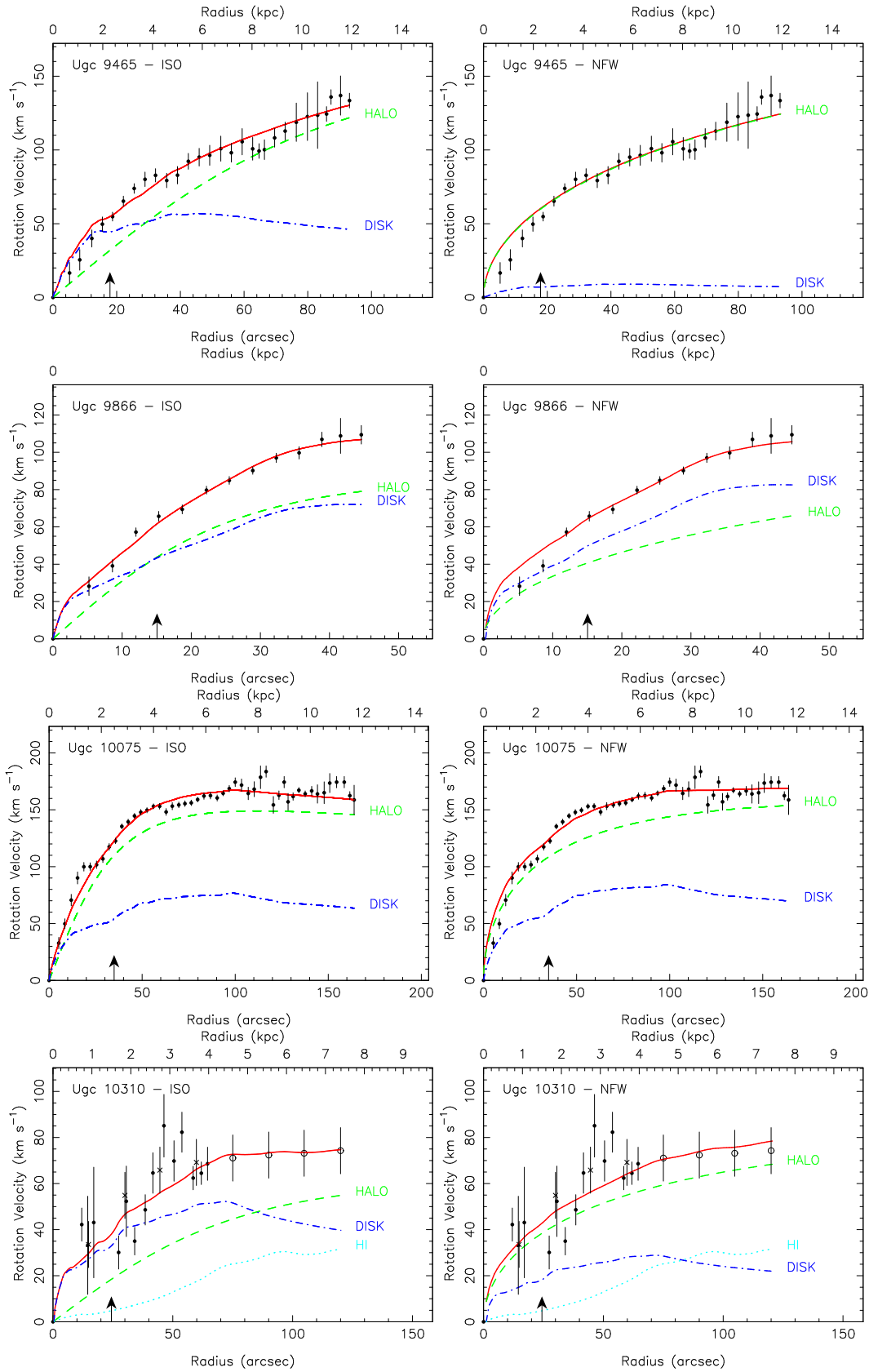


**Figure 13.** Best fit model for the rotation curve of UGC9465, UGC9866, UGC10075 and UGC10310 with isothermal sphere profile (left) and NFW profile (right). Dots are for optical velocities, open circles for HI velocities and crosses for HI in the central part, not taken into account. The arrow on the X axis indicates the disk scale-length.

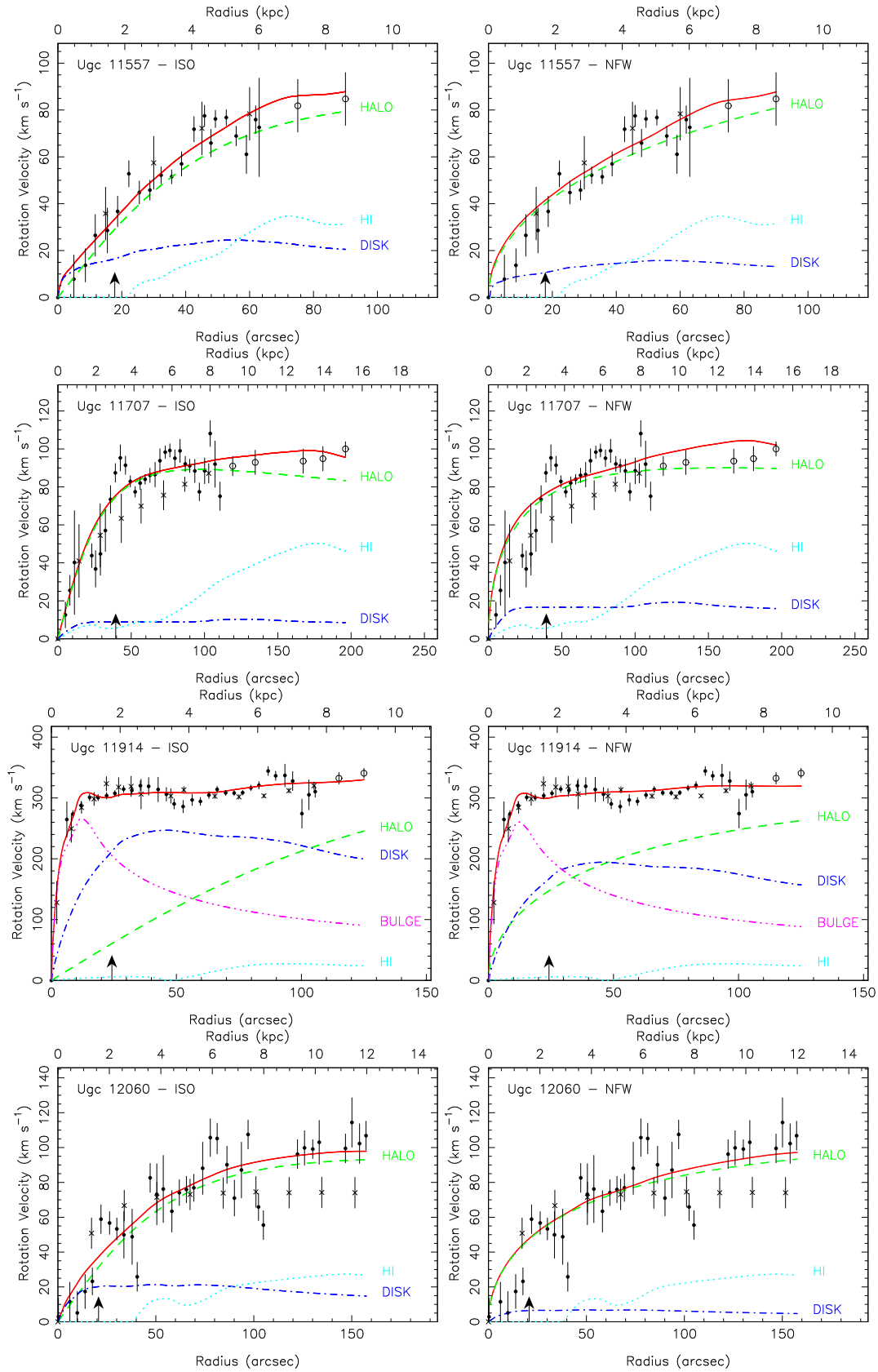


**Figure 14.** Best fit model for the rotation curve of UGC11557, UGC11707, UGC11914 and UGC12060 with isothermal sphere profile (left) and NFW profile (right). Dots are for optical velocities, open circles for HI velocities and crosses for HI in the central part, not taken into account. The arrow on the X axis indicates the disk scale-length.